BASIC RESEARCH IN CRYSTALLINE AND NONCRYSTALLINE CERAMIC SYSTEMS

Department of Materials Science and Engineering
Ceramics Division
Massachusetts Institute of Technology
Cambridge, Massachusetts 02139

ANNUAL REPORT

For the Period August 1, 1978 to October 31, 1979

Prepared for:

U.S. Department of Energy
Under Contract No. EY-76-S-02-2390

DISCLAIMER

BASIC RESEARCH IN CRYSTALLINE AND NONCRYSTALLINE CERAMIC SYSTEMS

Department of Materials Science and Engineering
Ceramics Division
Massachusetts Institute of Technology
Cambridge, Massachusetts 02139

ANNUAL REPORT

For the Period August 1, 1978 to October 31, 1979

Prepared for:

U.S. Department of Energy
Under Contract No. EY-76-S-02-2390

TABLE OF CONTENTS

Table of Contents (Continued)

INTRODUCTION

The Basic Research Programs in Ceramics sponsored by the U.S. Department of Energy supports a significant fraction of the research effort and graduate student training in ceramics at M.I.T. Various research subjects have been investigated in the past, including heat conduction, surface characteristics, diffusion in oxides, high temperature kinetic processes, microstructure development, effects of microstructure on properties, the structure and properties of noncrystalline ceramics, dissolution kinetics, materials preparation, and solid-vapor reactions. This report presents results of the current research program.

The program this year has been supervised by Professors W.D. Kingery, R.L. Coble and R.M. Cannon. The experimental work is performed largely by graduate students working toward advanced degrees, along with technicians and research staff. Supervising staff members and students are identified for each research project described in this report. All work has been planned by the Principal Investigators.

The importance of basic research programs in ceramics processing and properties is becoming widely recognized as the critical role of improved ceramic materials for energy systems is acknowledged. The needs identified in the 1977 series of workshops on DOE programs in energy-related materials research and by the ongoing efforts of the DOE Council on Materials Science are being translated into the basic and applied research necessary to fulfill the established objectives in the effort to solve the nation's energy problems. Present indications are that ceramics in numerous applications will be critical in meeting national energy requirements.

1.0 Electrical, Optical and Dielectric Properties

1.1 Electrical Conductivity in Single-Crystalline MgO

Personnel: D.R. Sempolinski and W.D. Kingery

The objective of this study is to define the defect structure of MgO through an examination of its electrical properties. To do this, it must be realized that MgO is a mixed conductor and that its defect structure is extrinsic in nature. These factors imply that any investigation of the electrical properties must emphasize the need to characterize both the mixed conduction phenomena and impurity effects.

In this study, this is accomplished by measuring the DC conductivity and the ionic transference number and by using samples which are doped so that only one solute controls the defect structure. With this approach, it is possible to examine the ionic and electronic conductivities individually and to assess the effects of specific dopants.

Measurements were made for temperatures of 1200 to 1600°C and oxygen pressures of 1 to 10^{-12} atm. The solutes considered are Fe, Al, Sc and Li.

The resulting ionic and electronic conductivities have several features which help to define the transport processes in MgO and provide the data needed to calculate a number of material parameters.

A) Ionic Conductivity and Mg Vacancy Mobility in MgO

Two characteristics of the ionic conductivity are evident from the data. First, the magnitude is directly proportional to the trivalent impurity concentration and, second, the activation energy is independent of the specific dopant. In every instance where ionic conduction is detected, the activation energy is 2.1 eV (±.15 eV).

These observations suggest that the ionic charge carrier is the same in each case and that it is a defect which is generated whenever trivalent solutes are introduced into the MgO. They can be explained if the ionic charge carrier is assumed to be the magnesium vacancy, V''_{Mg}. This defect is formed during the solution of any trivalent element, Im_{Mg}, into MgO:

$$Im_2O_3 \xrightarrow{MgO} 2Im^{\cdot}_{Mg} + V''_{Mg} + 3O_O$$

and, in the extrinsic regime, its concentration, as indicated by the charge balance condition:

$$[Im^{\cdot}_{Mg}] = 2[V''_{Mg}]$$

is directly proportional to the solute concentration.

Additional support for this interpretation comes from the conductivity data for the Li-doped sample. In this instance, ionic conduction is not observed. Since Li should suppress the magnesium vacancy concentration in MgO, this result is consistent with the idea that ionic conduction arises from V''_{Mg} motion.

This model of the ionic conduction mechanism leads to a direct determination of the diffusion coefficient of the magnesium vacancy, $D_{V''_{Mg}}$. Since the carrier concentration is known from the charge balance condition and the conductivity has been measured, the mobility term can be calculated and, through the Nernst-Einstein equation, used to compute $D_{V''_{Mg}}$.

When this exercise is performed (see Fig. 1), the following least-square fit expression is obtained:

$$D_{V''_{Mg}} = .38 \exp\left(\frac{-2.27\ eV}{kT}\right).$$

This result is consistent with several theoretical calculations which compute activation energies for vacancy motion of 2.1±.1 eV and it does provide an estimate for the entropy of motion term, $\Delta S_M/k \cong 4.1$. Moreover, this expression generates reasonable values for the diffusion coefficient of the magnesium ion, D_{Mg} (if magnesium vacancy levels of 100 to 2000 ppm are assumed). In fact, it appears from this calculation that the order of magnitude shutter in the measured values of D_{Mg} is due to differences in the background impurity levels of the starting materials.

B) Electronic Conduction and Deep Impurity Levels in MgO

The electronic conductivity also shows a distinct behavior. For every sample, except the Li-doped one, a p to w-type transition is observed as a function of oxygen pressure.

Not only is this P_{O_2} dependence consistent with the defect structure presented in the preceding section but, when considered from the viewpoint of the band gap structure, it provides a different way of looking at the prevailing charge balance condition. Since $Im^{\cdot}_{Mg}$ is an ionized donor state and V''_{Mg} is an acceptor level, the charge balance condition implies that compensation is occurring between these two types of states.

This process was particularly evident in the case of the Fe-doped sample. In the oxidized state, iron is mostly trivalent since one of its electrons has been used to fill the acceptor levels of the magnesium

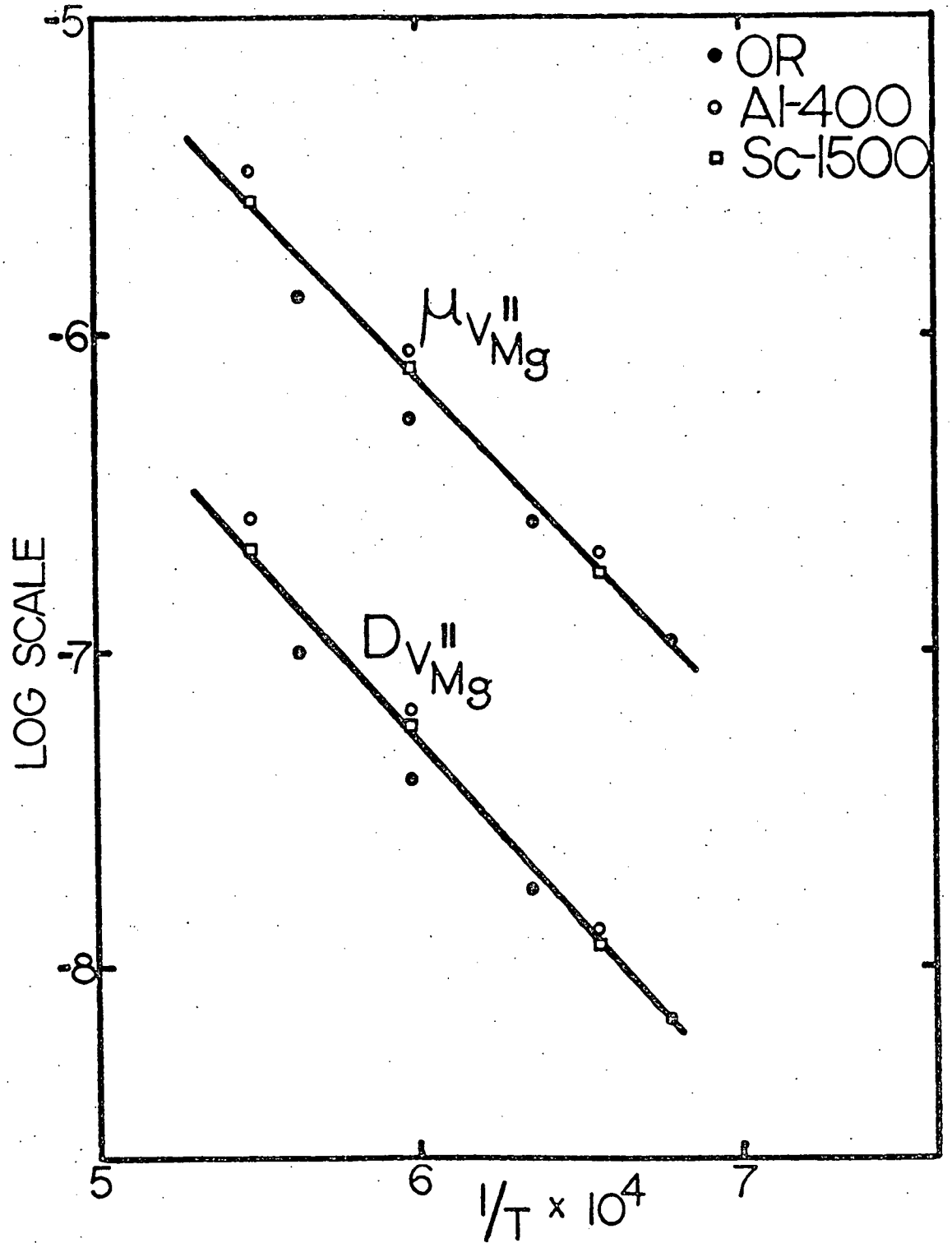

Fig. 1 Temperature dependence of mobility and diffusion coefficient of V_{mg}".

vacancies which are present. As the sample is reduced, however, the magnesium vacancies leave the system and the electrons associated with them now fill up the Fe^{x}_{Mg} states which in the absence of the V''_{Mg} acceptor levels become the lowest energy states available. This transition reflects the fact that as the ferric level moves toward the conduction band during the reduction process it passes the Fe^{x}_{Mg} level.

Several important material parameters were also determined from the electronic conductivity data. For a n to p-type transition, the temperature dependence of the electronic conductivity minimum is given by

$$\sigma^{min}_{elec} = 2e(\mu_p \mu_n N_V N_C)^{\frac{1}{2}} \exp\left(-\frac{Eg}{2kT}\right) ,$$

where μ_p and μ_n are the hole and electron mobilities, N_V and N_C the densities of states at the valence and conduction bands and Eg is the thermal band gap. Estimates for both $\mu_p \mu_n$ and Eg can be obtained by applying this expression to the electronic conductivity data.

The results of this calculation show that the thermal band gap in MgO is approximately 7.1 eV and, if the mobilities are assumed to be inversely proportional to their effective masses, at 1400°C the hole mobility is roughly 7 cm^2/volt sec and the electronic mobility is about 60 cm^2/volt sec.

The significance of these latter values is that they indicate that the electronic species are 10^8 more mobile than the magnesium vacancy. For the ionic and electronic conductivity to be approximately equal, therefore, the magnesium vacancy concentration must be 10^8 higher. This conclusion justifies neglecting the electronic species when formulating the charge balance condition.

1.2 Development of ITC Apparatus

Personnel: D.R. Sempolinski and W.D. Kingery

The ionic thermocurrent (ITC) experimental system provides a direct and concise method for studying defect associates in ionic materials. The activation energies for reorientation and the concentration of impurity-vacancy complexes can be determined by measuring the current which is generated during depolarization. These parameters can be obtained with a single ITC measurement, which is a marked improvement over such techniques as dielectric loss and internal friction experiments.

The requirements of the ITC method in regard to the sensitivity of the electrical measuring circuit and temperature control are, however, severe. The ITC apparatus must be able to detect currents of 10^{-11} to 10^{-13} amps and

permit rapid cooling of the sample while an electric field is being applied.

The original experimental system used in this study met the first requirement but not the second. The electrical noise was suppressed to approximately 7×10^{14} amp, but quenching of the sample could not be achieved even with the addition of cooling coils.

As a result, the ITC apparatus has been redesigned. A new hollow sample holder is being constructed which can be cooled directly using cold nitrogen gas, making sample quenching possible. To increase the efficiency of this operation, the sample holder is being made as small and as light as possible and is being enclosed in a vacuum chamber to thermally isolate it from any surrounding material which may retain excess heat. It appears that sample temperature as low as 120°K can be achieved with such an arrangement.

Although the initial purpose of this investigation was to study impurity-vacancy associates in MgO, it is hoped that once the ITC apparatus is operational a number of ionic material systems can be examined.

1.3 Vacuum Ultraviolet Properties of Aluminum Oxide and Their Relation to the Electrical Conductivity

Personnel: J.B. Blum and R.L. Coble

A facility was designed and constructed to perform near-normal incident optical reflectivity measurements in the vacuum ultraviolet spectral range at elevated temperatures. The reflectivity of undoped, single crystalline Al_2O_3 was measured, using this facility, from 9.0 to 12.5 eV. The measurements were performed at 25°, 275° and 450°C on samples of two different crystallographic orientations.

The room temperature results displayed a series of exciton peaks at 9.1, 9.5, 9.9 and 10.1 eV. The latter three peaks correspond to a Wannier model. Interband peaks were observed at 10.4, 11 and 12 eV. These results are consistent with a band gap of 10.3 eV at room temperature.

The spectra shift by -1.4×10^{-4} eV/K between 25° and 450°C, which was attributed to a decrease in the band gap of Al_2O_3 by this amount.

1.4 The Electrical Conductivity of Pure and Yttria-Doped Uranium Dioxide

Personnel: N. Dudney and R.L. Coble

Recent discussions of the defect structure of UO_{2+x} have assumed that defect clusters are formed due to the electrostatic interaction of uranium +5 ions and the negative oxygen interstitials. The proposed models differ

only in the size and effective charge chosen for the clusters. From conductivity measurements, if the hole mobility is known, the concentration of holes which are not bound to a defect cluster may be determined and compared to the proposed defect models.

Conductivity measurements of lightly doped urania were used to determine the hole mobility. Yttria was found to fix the concentration of holes, allowing the mobility to be calculated accurately. Yttria-doped urania was also studied to determine if yttrium significantly enhanced the concentration of vacant oxygen lattice sites and therefore the ionic conductivity of urania. If so, this would improve the properties of urania that are important for high-temperature solid electrolyte fuel cell applications.

The conductivity of dense polycrystalline urania was measured as a function of the oxygen partial pressure between temperatures of 800° and 1400°C. The composition was varied from about UO_2 to $UO_{2.1}$ using the thermodynamic data available in the literature. Conductivity measurements of yttria-urania solid solutions, with composition between 1/4 and 10 cation mole percent yttrium, were made over the same oxygen partial pressure and temperature ranges as for the pure material.

The conductivity of the pure urania increased rapidly with the oxygen partial pressure and was approximately proportional to the concentration of excess oxygen. Yttria enhanced the electronic conductivity of urania at lower oxygen partial pressures resulting in a conductivity that was independent of the oxygen partial pressure and proportional to the concentration of yttrium of to 1 mole percent. At higher oxygen partial pressures, the conductivity of the doped samples became equal to that of the pure urania.

Because the yttrium fixed the concentration of holes, the hole mobility was calculated from the conductivity. For the temperature range studied, the mobility is between 0.061 and 0.085 $cm^2/Vsec$ with an activation energy of 0.085 eV. Yttrium concentrations greater than 1 mole percent decreased the pre-exponential term of the mobility.

Assuming the hole mobility is the same in both the pure and yttria-doped samples, the concentration of holes in pure urania as a function of the composition and temperature was determined. The hole concentration was found to be proportional to the concentration of excess oxygen and the ratio of holes per excess oxygen atoms increased approximately exponentially with temperature from values less than 1 at 800°C to about 2 at 1400°C. The concentration of free holes is larger than predicted by the typical cluster models. The temperature dependence indicates that the defects become disordered at temperatures greater than about 1200°C. These results are not consistent with a Kröger-Vink type of analysis, which is based on an ideal

dilute solution approximation, of the observed oxygen partial pressure dependence for the conductivity.

No evidence of an anion deficient lattice or enhanced ionic conductivity for yttria-doped urania was found from these conductivity measurements, although this had been expected from lattice parameter and density measurements reported in the literature.

2.0 Kinetic Studies

2.1 Hydroxyl Processes in MgO

Personnel: K.W. Cheng and W.D. Kingery

MgO crystals containing hydroxyl ions have characteristic infrared absorption bands. Two of the best characterized bands are the 3296 cm^{-1} and the 3700 cm^{-1} bands. These were determined to belong to V_{OH^-} and Mg(OH) precipitates, respectively. Henderson and Sibley (J. Chem. Phys. 55, 1276 [1971]) studied the annealing characteristics of crystals containing OH impurities. They slow-cooled the crystals from 1010°C at a rate of 40°C/hr to room temperature. The crystals were then annealed for 10 min at 300°C and quenched. After IR measurements were made, the crystals were annealed and quenched at higher temperatures. These quenching studies were done in the temperature range of 300° to 1200°C. It was found that the relative absorptivity, R, of the 3296 cm^{-1} band can satisfy a functional form

$$\frac{R^2}{1-R} = \exp \frac{-\Delta H}{RT} \qquad (1)$$

with an activation energy of 1.42 eV. The 3700 cm^{-1} band can satisfy

$$1-R = \exp \frac{-\Delta H}{RT} \qquad (2)$$

with an activation energy of 0.45 eV.

The former reaction can be interpreted as the breaking up of OH V OH defects into V_{OH^-} and OH. The latter reaction can be interpreted as the dissolution of $Mg(OH)_2$ precipitates. There are doubts as to whether equilibrium can be obtained in these brief 10 min anneals. We repeated Henderson and Sibley's experiment with longer annealing times of 1 hr and 24 hr. The 3296 cm^{-1} band was found to obey Eq. (1) again with slightly different activation energies. The results of the three studies range from 1.13 to 1.42 eV. The 3700 cm^{-1} band, however, does not obey Eq. (2), thus casting doubt on the validity of this equation.

At temperatures higher than 1100°C, one would expect one V_{OH^-} to dissociate into V''_{Mg} and $OH^{\cdot}_{O}$. It was found that quenching above 1100°C resulted in irreversible loss of V_{OH^-}. This loss was previously interpreted by Harris and Crawford (Phys. Stat. Sol.(a) 35, 667 [1976]) to be due to the dissociation of V_{OH^-}. However, we found that this loss was diffusion controlled. The rate of loss of OH impurities was found to be the same as the oxidation rate of Fe in undoped Norton single crystals.

Annealing crystals containing hydroxyl impurities in reducing atmospheres results in H_2 bubble formation. This process was found to be diffusion controlled. The diffusivities reported by Briggs (Ph.D. thesis, University of Bradford) were found to be in fairly good agreement with the iron oxidation rate in undoped Norton crystals.

The formation of H_2 requires the reduction of $OH_O^{\cdot}$ by electrons. This loss of valence of $OH_O^{\cdot}$ has to be charge-compensated by the loss of cation vacancies. Therefore, this whole process is controlled by cation vacancy diffusion. Similarly, the loss of hydroxyl above 1000°C has to be accompanied by cation vacancy loss. The diffusivities of these two processes agreed with the rate of oxidation of Fe in undoped Norton crystals.

2.2 Kinetics of Oxidation Processes in MgO

Personnel: K.W. Cheng and W.D. Kingery

It has been generally accepted that oxygen is taken up during the oxidation of Fe^{2+} to Fe^{3+} with the creation of a cation vacancy for charge balance, i.e. $\frac{1}{2}O_2 + 2Fe_{Mg}^{x} \rightarrow 2Fe_{Mg}^{\cdot} + V_{Mg}'' + O_O$.

Reported literature data obtained by following the isothermal change in the concentration of Fe^{3+} showed they are diffusion-controlled. Reported oxidation data for nominally "pure" MgO have oxidation rates faster than would be expected if they were controlled by cation vacancy diffusion. However, Gourdin (Ph.D. thesis, M.I.T., 1977) had found that the oxidation rates of Oak Ridge crystals were much slower.

In our study, a Norton crystal, a deformed (by bending) Norton crystal, a hot-forged Norton crystal, an Oak Ridge crystal, a 310 ppm Fe-doped Spicer crystal and a 3250 ppm Fe-doped Spicer crystal were used. It was found that the rate of increase in Fe^{3+} in the Oak Ridge crystal was actually caused by iron contamination during the anneal; therefore, the extremely slow kinetics reported by Gourdin were actually a contamination rate. The 3250 Fe-doped sample was initially reduced in 10^{-7} atm of oxygen partial pressure. The rate of oxidation in 1 atm oxygen was monitored by following the isolated Fe^{3+} peak using EPR. In the temperature range between 1230° to 1540°C, $\tilde{D}$ was found to be 8 exp -2.65 eV/kT. MgO is a mixed conductor at these temperatures. $\tilde{D}$ can be shown to be equal to $3D_V\bar{t}_e$, where D_V is the cation vacancy diffusivity and $\bar{t}_e$ is the average electronic transference number. One can calculate a $\tilde{D}$ using the data reported by Sempolinski (Ph.D. thesis, M.I.T., 1979). The calculated values are in good agreement with the experimental $\tilde{D}$. This is consistent with many relaxation experiments with single crystals of transition metal oxides which indicate that changes

in defect concentration in those oxide crystals are accomplished mainly by volume diffusion of point defects to and from the crystal surface.

For the undoped Norton crystals, $\tilde{D}$ was found to be 100 exp -2.7 eV/kT for the temperatures from 940° to 1460°C. This rate was found to be the same for all the Norton crystals regardless of the amount of dislocations introduced by deformation. The large discrepancy between the two sets of data cannot be explained by defect association because defect association at these temperatures and concentration levels cannot possibly cause such a large difference in oxidation rates. There are data in the literature which indicate that oxygen can diffuse in the dislocation cores. Since the disorder in the dislocation core can act as a source or sink for vacancies, therefore, one would be led to believe that dislocations can enhance the oxidation rate. That is, oxygen will diffuse in the dislocation core from the crystal surfaces, and the cation vacancies will diffuse into the bulk of the crystal from the dislocation core. Therefore, the presence of dislocations would effectively shorten the diffusion distance of the cation vacancies. Using this as a model for enhancement, one can estimate the time required for cation vacancy equilibration. Taking the time for equilibration to be approximately equal to ℓ^2/D_V, where ℓ is the half distance between the dislocations, the time required to equilibrate at 1400°C for a crystal containing $10^6/cm^2$ dislocation density is about 1 sec. That is, for all practical purposes, the equilibration can be achieved instantaneously. So, the rate-limiting step is the oxygen pipe diffusion. The dislocation densities in the undoped Norton crystals are all above $10^6/cm^2$; therefore, the $\tilde{D}$ obtained can be interpreted as a measure of the oxygen pipe diffusion.

This interpretation contradicts the conclusions drawn from the results of the 3250 Fe-doped sample. Furthermore, etching study on the iron-doped sample revealed a dislocation density similar to the Norton crystals.

The fundamental assumptions in the dislocation enhancement model are that the dislocation can transport oxygen and can be a source and sink for cation vacancies. If, however, the dislocation pipe can only act as a finite source and sink for vacancies, it is obvious then that the validity of the dislocation enhancement model depends on the number and distribution of the dislocations and also on the amount of vacancies required for equilibration. Having these additional constraints on the dislocation enhancement model, the above discrepancy may be explained as follows. The dislocation can generate enough vacancies to oxidize completely the Fe ions in the undoped Norton crystals, whereas, for the 3250 Fe-doped crystal, the dislocation pipes cannot provide an adequate amount of vacancies to oxidize

completely the Fe ions. Therefore, the majority of the vacancy relaxation takes place only at the crystal surfaces.

The critical test of this model is to hold the dislocation density constant and vary the amount of Fe to be oxidized. A series of oxidation experiments were done on a 3250 Fe-doped sample at 1422°C. The results are as follows:

	Reduced at	Oxidized at	Amount of Fe Oxidized	$\tilde{D}$
1	5×10^{-10} atm O_2	10^{-7} atm O_2	64 ppm	5.6×10^{-7} cm^2/sec
2	10^{-7}	5×10^{-5}	633	4.6×10^{-7}
3	5×10^{-10}	5×10^{-5}	697	2.0×10^{-7}
4	10^{-7}	1	2532	2.0×10^{-7}

This supports the above conjecture. Oxidation in oxygen of a previously 10^{-7} atm-reduced 310 Fe-doped sample gave a diffusivity intermediate between the undoped Norton and the 3250 Fe-doped sample data.

2.3 Hot Stage SEM Study of Microstructure Development

Personnel: E. Giraldez and W.D. Kingery

For chemically prepared powders such as magnesium oxide, a magnesium hydroxide precipitate is normally prepared and calcined at a temperature of about 900°C. During the calcination process involving the transformation of the hydroxide to oxide, various physical-chemical processes including crystallite formation and grain growth occur.

The dehydration process for single crystals has been characterized by many different techniques. The transformations taking place in powders have been much less studied. The factors which affect the morphology between the dehydration temperature and the calcination temperature are not well understood. It is believed that the residual surface hydroxide, surface diffusion, evaporation condensation or any other initial-stage sintering process are all related to the morphology changes.

In order to investigate the microstructure development taking place and to relate it to a particular process during the transformation of the hydroxide to oxide, a hot stage to be used with a scanning electron microscope is being developed. The advantage of the SEM over the optical microscope is the fact that a higher resolution, greater depth of field and higher magnifications are obtained. The principal drawback is that the sample being used has to be conductive. The materials that we will study are insulators; to overcome the problem of charging a low accelerating

voltage (between 5 and 10 kV) will be used, which is the region where the secondary electron generation coefficient is greater than one. A problem with using the low accelerating voltages is that resolution decreases, but it still will be an order of magnitude better than that of optical microscopy. The hot stage will be operable to temperatures as high as 1600°C, well above the calcination temperature of most hydroxides.

2.4 Aging Processes During Precipitation, Storage and Calcination of Magnesium Hydroxide

Personnel: A.F. Henriksen and W.D. Kingery

Interest in the manufacture and use of fine powders (<1 μ G.S.) in ceramic processing has gained momentum within the past few years. The demand for high density, flawless, polycrystalline ceramics is on the rise in high-technology energy-related products. It has long been recognized that the most important stage in a process which begins with a powder is the perfection with which the unfired item can be produced, as any irregularity at that stage is enhanced during firing. Thus it is necessary to be able to control grain size, agglomeration behavior, flow characteristics, etc., in the initial powder.

Submicron size powders are usually manufactured by building up small particles from atomic size. One method of doing this is by precipitation processes, and a vast amount of research has gone into such methods. However, it is very difficult to characterize, much less control, the multitude of parameters which enter into a given precipitation process. The reason for this may lie in the fact that almost all research on precipitation processes focuses attention on the final powder, often after it has undergone calcination. Very little information exists on the effect of varying parameters upon the intermediate stages of the precipitation process.

We have developed a process consisting of a continuous backmix flow reaction which consistently yields uniformly sized $Mg(OH)_2$. This experimental set-up allows us to monitor the development of grain size and agglomerate size at any stage of the precipitation process. At the same time it is possible to control parameters such as nucleation rate, growth rate and agglomeration rate on a steady state basis.

It is our aim to monitor the precipitation process during its different stages and to relate the observations to the change in external parameters. Furthermore, the effect of storage of $Mg(OH)_2$ on the development of agglomerates will be monitored, and finally, with the aid of a hot stage in the SEM, we will investigate the effect of the calcination process.

2.5 Oxygen Diffusion in Doped and Deformed Magnesium Oxide

Personnel: A.F. Henriksen and W.D. Kingery

Though the diffusion coefficient of oxygen in MgO has been reported by a few researchers, there remains controversy with respect to the mechanism of oxygen diffusion. It is generally agreed that the diffusion of oxygen is slow through the lattice, being about two orders of magnitude slower than the diffusion of Mg at the same temperature. Creep data and results from experiments on O^{18} exchange using polycrystalline MgO suggest that oxygen diffuses much faster along grain boundaries than through the bulk, and recent speculation has yielded the result that oxygen may diffuse faster than hitherto assumed through the bulk via pipe diffusion. Regardless of how present data are interpreted, it seems clear that no single theory regarding the mechanism of oxygen diffusion in MgO prevails.

Part of the reason for this ambiguity lies in the methods which have been used to date to measure oxygen diffusion. The traditional electron microprobe method cannot be used and the available active oxygen isotopes are too short-lived to make tracer experiments possible. With the emergence of the SIMS, however, it is now possible to analyze concentration gradients using the stable oxygen isotope O^{18}. Furthermore, due to the high spatial resolution of the SIMS it is not necessary to achieve a very deep penetration of the diffusing species, so experiments on single-crystal MgO using a thin-film technique become practical.

Some work has already been done on oxygen diffusion in high purity single-crystal MgO and Al_2O_3 using thin-film technique combined with SIMS analysis. However, indications are that the inherent impurity level in even the best available MgO single crystals are of such magnitude that it is doubtful that it is intrinsic diffusion which is being measured. As a consequence, we have chosen to measure the oxygen diffusion in Sc-doped MgO where recent studies have shown the resulting defect structure to be well characterized. If oxygen diffuses via a vacancy mechanism it would seem possible to affect the mobility of oxygen by lowering the concentration of oxygen vacancies by adding trivalent cation impurities. To shed some light on alternative diffusion mechanisms such as the suggested pipe diffusion model, we propose to conduct an oxygen diffusion experiment using a single crystal of MgO which has been heavily deformed by hot pressing.

2.6 Defect Equilibria and Precipitation Phenomena in $SrCl_2$-Doped KCl

Personnel: T.R. Gattuso and R.L. Coble

In attempting to study the slow defect diffusivity in KCl using density and density relaxation measurements, we were unexpectedly thwarted by the finding that quenched crystals were more dense than slowly-cooled specimens, but would recover, upon low-temperature annealing, to give density values equivalent to those of the "annealed" specimens. We have been unable to explain this phenomenon although all possible side-effects of which we are aware have been considered. Initially, we simply assumed that Schottky defects were dominant, and that vacancy pairing gave additional measureable contributions to the diffusive transport, but not to the electrical conductivity; these results are available from several previous investigations that are seemingly self-consistent. Thus, we had assumed that excess vacancies would be retained on quenching, and, from earlier investigators' data, the concentrations should have been large enough to be readily measureable.

In considering the effect opposite in sign to that expected, we have considered dislocation effects and vacancy pairing upon cooling and have generated a model for vacancy pairing as a function of cooling rate and a model for pair transport. We have been led to the conclusion that even in the highest purity crystals available impurity effects and association and precipitation phenomena are important. Because of an inability to resolve the problems associated with the "pure" material, we have opted for selective, low-level doping to study the material, and have adopted conductivity measurements because of their greater sensitivity to the variety of effects of interest.

Among the attractive features of the alkali halide systems is the presumed ability to produce controlled concentrations of extrinsic defects by means of divalent cation additions. Most defect studies such as ionic conductivity, dielectric loss and ionic thermal current measurements are carried out without regard for the phase transformations which can occur in these binary systems. In particular, precipitation is often ignored, or when it is considered the details of the nucleation process, precipitate morphology and growth kinetics are frequently glossed over. Few systems have been investigated in detail and, in general, the solubility data are not available.

We have recently begun an investigation of the KCl-$SrCl_2$ system, or more precisely, the KCl-K_2SrCl_4 sub-binary. Since the ionic conductivity is a sensitive function of the amount of Sr^{++} in solution, we are employing

isothermal conductivity relaxation after various heat treatments to study the kinetics of precipitate nucleation, growth, and re-solution. Single crystals of KCl with up to 1 mole% $SrCl_2$ in solution were grown by the Czochralski method in a reactive gas atmosphere (HCl) to ensure removal of oxygen and water. We find that above the solvus temperature, the equilibration times as indicated by the relaxation in conductivity after step changes in temperature are very short. Below the solvus temperature, the equilibration times vary between hours and weeks at the same temperature depending on heat treatment. Crystals cooled from the solid solution region to aging temperatures well below the solvus show very long relaxation times. Optical microscopy reveals that in these crystals nucleation occurs only at the free surface and precipitation proceeds by growth of blade-like particles along preferred directions into the bulk. From these observations a significant barrier to nucleation caused by strain energy associated with the precipitate may be assumed. Upon cooling from the solid solution region to room temperature, copious precipitation occurs in the bulk in the form of fine, equiaxed, uniformly distributed particles. On reheating and aging within the two-phase region, blades nucleate on these particles and grow. Equilibration times are relatively short after this treatment.

There are no X-ray data available for the K_2SrCl_4 phase, but comparison of diffraction peaks from aged single crystals with polycrystalline material containing 30% eutectic indicates that the blades are the stable end member of the sub-binary. It is not known yet whether the precursor is the same phase. Work is underway to establish the crystal system and lattice parameters of the precipitate and the crystallographic relations between the precipitate and the KCl matrix.

Upon considering the phase equilibria in relation to the presumed Schottky defect formation (Fig. 1), it is possible to anticipate finding behavior that has not been discussed in the literature. We assume that the equilibrium concentration of Schottky defects is probably less than the maximum solubility of the solute at the eutectic temperature; the curve for the vacancy concentration as a function of temperature then crosses the solidus line somewhere between the eutectic temperature and the melting temperature of the pure solvent, (X_{BC},T). For temperatures above this point the solvent is intrinsic but may be in the two-phase region (liquid droplets). It could also be 1 ϕ intrinsic for a temperature interval fixed by X_B if $X_B < X_{BC}$. If $X_B > X_{BC}$ but less than the solubility limit at the eutectic, there is a temperature range in which the extrinsic behavior would be governed by the concentration of the second component that at equilibrium would be governed by the solidus line. All of those compositions would also

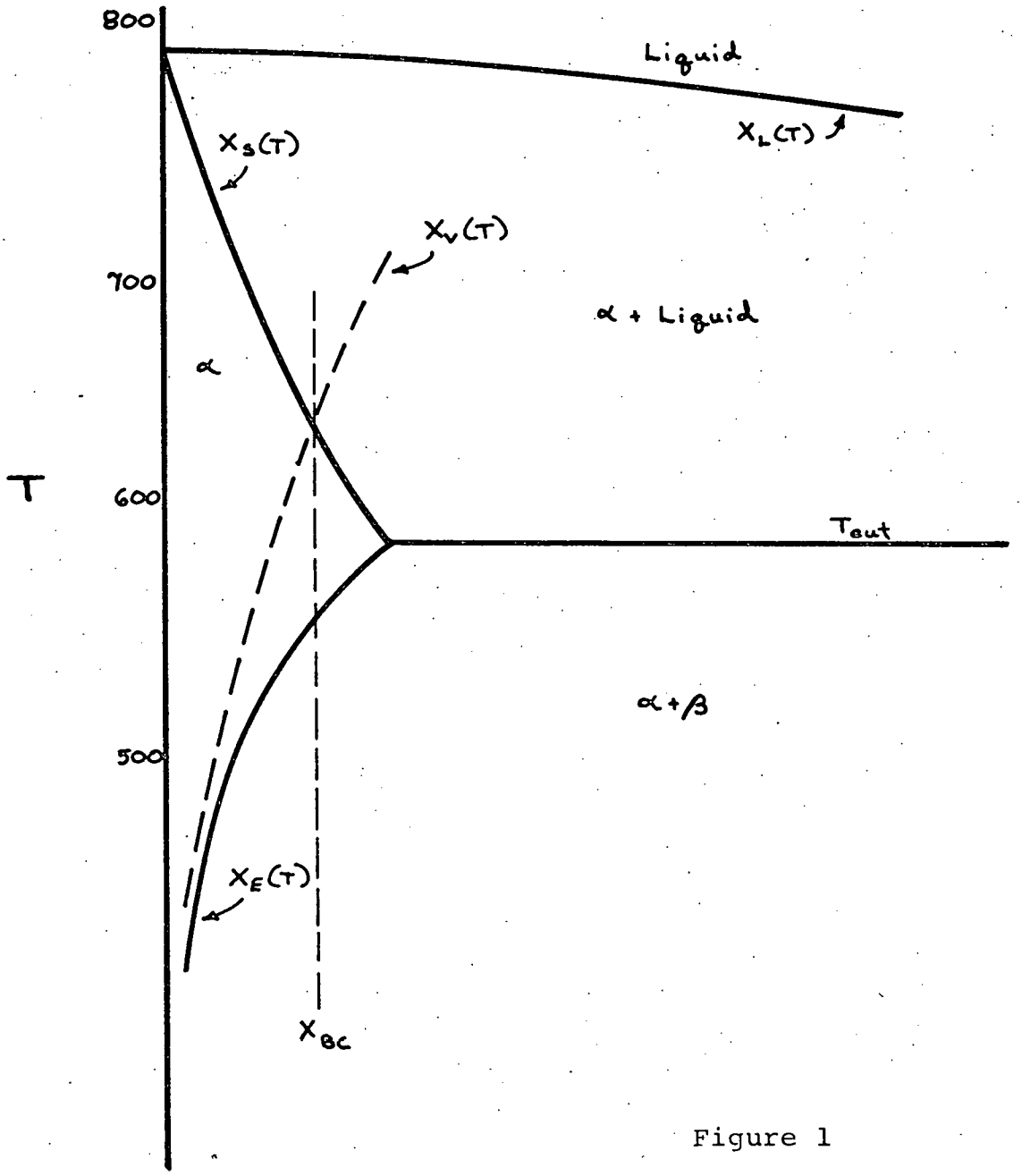
800
700
600
500
T
Liquid
$X_L(T)$
$X_S(T)$
$X_V(T)$
α + Liquid
α
T_{eut}
$\alpha+\beta$
$X_E(T)$
X_{BC}

Figure 1

become intrinsic at temperatures above (X_{BC},T). These samples would exhibit (σ,T) behavior somewhat like a semi-conductor in the exhaustion range rather than the usual behavior expected for extrinsic-intrinsic transitions in a single-phase region as a function of dopant content. This could lead to a misinterpretation of the temperature dependence, i.e., to associate it with the activation energy for defect migration rather than with that plus the temperature dependence of the solidus. The main points to be made are that the sample could be intrinsic although in a two-phase region, and that the conductivity temperature dependences for composition near the solubility limit will show characteristic differences that can be used to provide information concerning the location of the solidus with respect to the Schottky equilibria. At temperatures somewhat below the eutectic temperature the extrinsic behavior would be governed by association phenomena and then precipitation for control of the second component for temperatures below the solvus.

2.7 Quenching of Lattice Defects in KCl

Personnel: T.R. Gattuso and R.L. Coble

In the quenching and annealing experiments performed on metals in the late 1950's and early 1960's it was found that as the concentration of excess defects increased the relaxation kinetics became more complex and could only be described in terms of clustering of free vacancies into pairs, and in some cases higher order clusters, during quenching. Because of the strong, long-range, electrostatic interactive forces between defects in ionic crystals compared to the weak, short-range, elastic interactive forces between defects in metals, the pairing of defects during cooling is expected to be much more important in ionic materials.

The predominant point imperfections in KCl are separated Schottky defects and neutral vacancy pairs (anion and cation vacancies on adjacent lattice sites). At equilibrium the relative concentrations of these defect species are given by a mass action expression

$$\frac{[(V'_K V^{\cdot}_{Cl})^*]}{[V'_K][V^{\cdot}_{Cl}]} = K(T) = 6 \exp \frac{(\Delta h_b)}{kT} \qquad (1)$$

where Δh_b is the vacancy pair binding energy. We have modeled the evolution of the point defect population in KCl crystals during rapid cooling allowing migration of both separated and neutral, bound pairs to sinks and interaction between the two defect species.

A crystal at equilibrium at T_m contains n_m separated Schottky defects

and p_m neutral vacancy pairs. If the crystal is rapidly cooled and randomly distributed, fixed sinks operate, the excess defect concentrations (the differences between the actual and equilibrium values) are given by:

$$\frac{dn}{dt} = \frac{d}{dt}(n_m - n_{eq}) - \frac{n}{\tau_n} - \phi_A \tag{2a}$$

$$\frac{dp}{dt} = \frac{d}{dt}(p_m - p_{eq}) - \frac{p}{\tau_p} - \phi_A \tag{2b}$$

where n and p are the excess concentrations of separated Schottky pairs and neutral vacancy pairs, respectively; n_{eq} and p_{eq} are the respective equilibrium concentrations, both of which are functions of temperature only. The τ's are relaxation times and the assumption of first order kinetics is appropriate for the cylindrical geometries associated with dislocations which we presume act as perfect sinks. The form of τ is λ^2/D where λ is the sink spacing and D the appropriate defect diffusivity. For separated pairs the slower anion vacancy controls the relaxation time and τ is a simple Boltzman factor. The diffusion of the bound pair is more complex and a pair association calculation for the tight binding case gives:

$$D_p = \frac{4a^2 w_1 w_2}{3(w_1+w_2)} \tag{3}$$

where a is the anion-cation separation; w_1 and w_2 are the frequencies of anion and cation jumps into the pair. Both w_1 and w_2 are exponentially dependent on the temperature. ϕ_A is the rate at which separated pairs disappear by combining to form bound pairs. ϕ_A is also the rate at which bound pairs are produced by the association reaction since no defects are created or destroyed in the reaction.

Adding (2a) and (2b) eliminates ϕ_A and gives an equation for the total excess defect concentration, but more must be known about the relative concentrations of separated and bound pairs in the supersaturated crystal before a solution can be obtained. Although the crystal is kinetically limited from maintaining overall equilibrium during rapid cooling, a reduction in free energy results from the formation of neutral vacancy pairs from separated Schottky defects. Given the short distances between defects compared to the distances between sinks and the strong electrostatic attraction between defects of opposite sign, it is not unreasonable to assume local equilibrium between free and associated vacancies.

We have solved (2a) and (2b) numerically for the case of local equilibrium and hyperbolic cooling. The form of the total defect concentration versus time curves are similar to those for the case where association is

neglected but differ in that the defect population is dominated by neutral vacancy pairs. Initially, both separated and bound pairs are lost to sinks. As the temperature and consequently the defect mobilities fall, the total loss rate decreases and the total concentration levels off at a constant value. The concentration of separated defects continues to fall, however, as a result of the association reaction and the concentration of neutral, bound pairs passes through a minimum during cooling. At high cooling rates the final defect concentration depends strongly on the quench temperature, T_M, and weakly on the cooling rate. As the cooling rate is decreased the relative strengths of these dependences is reversed; the final defect concentration becomes strongly dependent on cooling rate and essentially independent of T_M.

The results of these calculations are in fairly good agreement with the few reported quenching experiments for ionic materials. Reports of excess ionic conductivity in quenched KCl imply an excess free vacancy fraction of about 10^{-7} (Ewles and Jain, Proc. Roy. Soc. A243 [1957]), but the conductivity is insensitive to the dominant defect. Density measurements on quenched KCl (Pellegrini and Pelsmaekers, J. Chem. Phys. 51, 5190 [1968]) indicate total defect concentrations of about 10^{-4}, in agreement with our calculations, and a dependence on T_M also in accord with our model.

2.8 The Origins of Internal Stresses in Polycrystalline Al_2O_3 and Their Effects on Mechanical Properties

Personnel: J.E. Blendell and R.L. Coble

A model for the stresses arising from thermal expansion anisotropy during cooling polycrystalline materials has been developed. The model incorporates the relaxation of stresses at high temperatures by diffusional creep with the generation of stresses due to thermal expansion differences across a grain boundary. The room temperature stresses are a function of grain size and cooling rate, which was assumed to be linear. It was found that the calculated room temperature stresses significantly increase with grain size and cooling rate. From the results of the calculation, an effective lower limit for stress relaxation could be defined. Using this effective lower limit and a linear dependence of stress on temperatures below the limit yields a simple method for estimating the room temperature stress.

The stresses were measured directly by a spectroscopic technique and inferred from measurement of the toughness. The samples were commercial Al_2O_3 which were annealed at 2150°K for various times and cooled at different linear rates.

While no grain size dependence of the stresses was observed, the cooling rate dependence was clearly demonstrated. The magnitude of the stresses measured by the spectroscopic technique were in good agreement with the value predicted from the model. There exists at present no agreement in the literature on the effect of thermal expansion stresses on the toughness. Thus, the observed increase in the toughness with increasing stress could not be used to determine the magnitude of the stresses.

The room temperature stresses can be minimized by slow cooling in the range of temperature where stress relaxation has been shown to be important.

3.0 Defect Structures, Defect Interactions, Grain Boundaries and Surfaces

3.1 Influence of Grain Boundaries on Electrical Conductivity in MgO

Personnel: D.R. Sempolinski and W.D. Kingery

This project is an extension of the electrical conductivity studies which have been performed on single crystalline MgO. The bulk properties have now been characterized well enough so that the role of grain boundaries in the conduction process can be assessed.

The approach taken in this investigation is the same as the one used in the single crystalline case. Measurements of both the DC conductivity and the ionic transference number are made on polycrystalline samples which have been doped so that only one solute controls the defect structure. The dopant levels are the same as those used in the single crystalline study so that any change in the electrical properties of the polycrystalline samples can be attributed to the presence of grain boundaries.

The solutes being considered are Fe and Sc. The samples are prepared by co-precipitation of the appropriate hydroxides followed by calcination, pressing and then sintering at 1600°C for 4 hr.

Initial results for a Fe-doped polycrystalline sample indicate that the activation energies for conduction are 3.05 eV at high temperatures (>1250°C) and 2.64 eV at low temperatures. These values differ from those seen for a Fe-doped single crystalline sample, which implies that different conduction mechanisms are operative in the polycrystalline case.

3.2 Scanning Transmission Electron Microscopy Investigation of Grain-Boundary Segregation in a ZnO-Bi_2O_3 Varistor

Personnel: W.D. Kingery, J.B. Vander Sande and T. Mitamura

Zinc oxide containing small amounts of bismuth oxide is one of several materials which exhibit a highly nonlinear current-voltage characteristic, which was at first interpreted as resulting from separation of the ZnO grains by a thin continuous intergranular phase. The present work was conducted with a field-emission-source scanning transmission electron microscope (STEM), which operated in the image and the energy dispersive X-ray microanalytical modes. Since the STEM has high spatial-resolution-microanalysis capabilities, it has many advantages. The present model uses a field emission gun as an electron source, resulting in a fine electron probe ($\sim$5 Å in diameter) with a large ($\sim 10^{-9}$ amp) current. This

combination of fine probe size and large current allows for high spatial-resolution-compositional analysis while maintaining a good signal-to-noise ratio in the microanalytical signal. In addition, the object chamber vacuum is routinely in the 10^{-9} torr range, ensuring operation in an environment where the instrument is not contributing to sample contamination, an otherwise difficult problem when stationary fine electron probes are used for high spatial-resolution-compositional analysis in a poor-vacuum instrument.

The sample examined was ZnO containing 0.04 wt% bismuth oxide. The grain boundaries contain many precipitate particles with a finite dihedral angle along with regions free from visible precipitates up to the highest magnifications used (x500,000). Typical traces taken across a precipitate-free boundary and across a small precipitate particle in the boundary indicate that the precipitate particles have a high Bi content relative to the matrix and that there is a region of Bi segregation adjacent the boundary independent of a second phase. Thus our observations agree with those of the finite dihedral angles previously observed and the absence of a continuous second phase. However, there is also a continuous region of substantially enhanced Bi concentration at all grain boundaries, so that a continuous compositionally altered boundary is present.

If Bi enters the ZnO structure in substitutional solid solution, replacing a divalent zinc ion with a trivalent bismuth ion corresponds to an extra positive charge in the 50-Å wide space-charge layer adjacent the boundary. For charge neutrality, this substitution corresponds to a negative charge at the boundary.

3.3 Boundary Segregation of Ca, Fe, La and Si in MgO

Personnel: W.D. Kingery, T. Mitamura, J.B. Vander Sande and E.L. Hall

Changes in the composition of oxide materials at and near boundaries have been reviewed by Kingery [J. Amer. Ceram. Soc. 57 (1974) 74]; the surface and grain boundary segregation of aluminum in MgO crystals resulting from spinel precipitation has been reported [W.D. Kingery et al., J. Amer. Ceram. Soc. 58 (1975) 239; C. Berthelet et al., Ceram. Int. 2 (1976) 62]. Johnson et al. [in "Grain Boundaries in Engineering Materials," J.L. Walter et al. (eds.), Claitors Publ. Civ., Baton Rouge, 1975] investigated grain boundary segregation in MgO by Auger electron spectroscopy and reported that segregation of Ca, Si and Ti occurred. Black and Kingery [J. Amer. Ceram. Soc. 62 (1979) 176] have reported surface segregation of ferric iron, chromium and scandium in single crystal MgO. In the present study we have investigated

grain boundary segregation in a sample of MgO, prepared by W. Coblenz, which contained small amounts of Fe, Ca, Si and La with the use of a "dedicated" scanning transmission electron microscope.

A sample of high purity MgO, prepared by autoclave oxidation of Mg metal at the General Electric Co. Glass Research Laboratory in Cleveland, and an admixture of ferrix oxylate were calcined at 700°C for 1 hr. Samples were pressed with oleic acid and isopropyl alcohol and subsequently sintered at 1700°C for 5 hr, annealed at 1100°C for 19 hr and air quenched by dropping from the furnace onto a bed of sand.

The samples were mechanically thinned by grinding to a final thickness of about 2 μm and then prepared for electron microscopy by ion thinning with argon ions accelerated through a potential of 6 kV. Conductivity in the electron beam was assured by coating the samples with a layer of evaporated carbon.

The samples were observed and X-ray microanalysis was carried out in a VG HB5 scanning transmission electron microscope manufactured by Vacuum Generators Microscopes Ltd., East Grinstead, England. A sample of a grain boundary was examined in which the bright-field image showed no indication of precipitation at a magnification of x200,000. High spatial resolution X-ray microanalysis was used to examine solute segregation. The spatial resolution is determined by the initial probe size, by the amount of beam spreading in the sample and by specimen stability during measurements. We estimate that sample stability and beam broadening limited the X-ray spatial resolution to about 50 Å.

For analysis, specimens were held in a graphite-nosed cartridge which allowed translation and tilting and the analysis was performed with a probe of about 25 Å diameter with a current of about 10^{-8} amps, which was manually stepped along a line perpendicular to the boundary. The foil was tilted such that the boundary was parallel to the electron beam. A 30 sec count time was used for each point and after collection a computer generated semispectrum.

Spectroscopic absorption analysis indicated that this sample contained 1570 ppm by weight Fe and 20 ppm by weight Ca. Emission spectroscopic analysis indicated the presence of 10 to 50 ppm by weight Si and less than 50 ppm by weight La. The projected grain boundary image is precipitate-free and about 40 Å wide. There is a substantial enhancement in concentration at the grain boundary over a region less than about 200 Å in width for each of the cations present. The relative enhancement of Si, Ca, and La is greater than that for Fe. This probably results because there is a greater strain energy contributing to segregation for these materials.

With experimental data now indicating segregation of aluminum, ferric iron, scandium, titanium, silicon, calcium, and lanthanum, it seems clear that segregation of solutes at grain boundaries in ionic oxides such as MgO is very common indeed, and that this factor must generally be taken into account in discussing properties and behavior of this class of materials.

3.4 Segregation of Aliovalent Solutes Adjacent Surfaces in MgO

Personnel: J.R.H. Black and W.D. Kingery

In the present study ion microprobe mass spectroscopy was used to investigate segregation effects in a 1000 Å layer adjacent a {100} surface of single crystals of MgO containing additions of Fe^{2+}, Fe^{3+}, Cr^{3+}, and Sc^{3+}, all within a single-phase concentration region.

Most of the measurements were made with samples from a single crystal (4N MgO from an ingot described as containing 2300 ppm Fe). Neutron activation analysis and absorption spectroscopy gave a cation fraction of 3200±200 ppm Fe. Another higher-iron-content crystal was analyzed as containing 4600±300 cation ppm Fe. Analysis showed that these samples contained <5 ppm each of Cr, Mn, Si, and Al. Some measurements were also made on a 4N MgO supplied as containing 800 ppm Cr (not analyzed by the present writers). High-purity crystals were cleaved and a layer of Sc_2O_3 was evaporated on the surface and diffusion-annealed for 48 hr at 1800°C. Wet chemical analysis indicated 3000 cation ppm Sc.

All samples were prepared by cleaving to expose a {100} surface which was chemically polished in 160°C phosphoric acid, then rinsed in distilled acetone and isopropyl alcohol. After heat-treating at a specified temperature for 3 hr, samples were either "slow-cooled" at a rate of 30°C/min, "intermediate-cooled" at 490°C/min, "air-quenched" by dropping from the furnace onto a bed of sand, or "liquid nitrogen-quenched" or "oil-quenched" by dropping from the furnace into a liquid nitrogen or oil bath. The last two are believed to be equivalent; the fall time, ∿0.3 sec, gave a cooling rate of ∿500°C/sec.

It was shown experimentally: (1) There is segregation of Fe^{3+}, Sc^{3+}, and Cr^{3+} in a region a few hundred angstroms (or less) thick adjacent a {100} surface of a quenched MgO crystal; (2) the amount and thickness of this segregation decrease as the quench rate increases; (3) no segregation is observed for Fe^{2+}; and (4) for Fe^{3+} and Sc^{3+} the total amount of segregation increases as the temperature decreases.

Segregation to surfaces can result from strain-energy effects, which are weak in experimental studies of $MgFe_2O_4$ nucleation from MgO (i.e.

homogeneous nucleation is inferred) and are unlikely for Fe^{3+} as a solute here. Strain-energy effects are even more unlikely for Sc^{3+}, which has almost the same ionic radius as Mg^{2+} (0.73 vs 0.72 Å), a closer value than that of Fe^{2+} (0.77 Å), which shows no segregation.

Segregation near surfaces can be caused by precipitation. However, the solubility of iron oxide in MgO in air, Cr_2O_3 in MgO, and the even larger solubility of Sc_2O_3 in MgO exclude this possibility for the quenched samples. In addition, the thin layer of segregation in the quenched samples is different from that found with surface precipitation processes.

Boundaries in MgO have a negative charge, and segregation near surfaces can result from the formation of a space-charge layer (resulting from a lower free energy of cation vacancy formation than that for anion vacancies, which is generally assumed for MgO, together with the presence of aliovalent solutes). This cause of the segregation agrees with the presence of Fe^{3+}, Cr^{3+}, and Sc^{3+} and the absence of Fe^{2+}, with the increased segregation observed at lower temperatures, and with the segregation width being less than hundreds of angstroms. For the relatively high aliovalent ion concentration in these samples the calculated value of the boundary thickness (tens of angstroms) is less than the measured value (hundreds of angstroms) which should be considered as an upper limit only. The difficulty in precisely locating interfaces and possible shifts during cooling preclude conclusions based on the shape or precise width of the segregation region.

It is tempting to consider a naive calculation in which the excess Fe^{3+} would be taken as a measure of the positive charge near the surface, i.e. corresponding to the oxygen excess at the surface. We have not done so because the oxidation of iron is not complete, because some fraction of the ferric ions are associated with magnesium ion vacancies to form associates (although calculations based on estimates of the binding energy indicate that isolated ferric ions are the major species in an air atmosphere at ≥1000°C), because the binding energy of the defect species at the surface is unknown, because a continuum calculation in the near-surface region may be inappropriate, and because there may be changes in solute distribution occurring during the quench. Much more information is required before a plausible quantitative treatment of the data can be attempted.

3.5 The Defect Structure of MgO Containing Trivalent Cation Solutes: Shell Model Calculations

Personnel: W.H. Gourdin and W.D. Kingery

We have used the Harwell Automatic Defect Evaluation System (HADES) program to calculate the energies of various defect aggregates found in MgO containing Al^{3+} and Fe^{3+} solutes and compensating cation vacancies. Calculated energies of substitution are compared with heats of solution derived from phase-diagram data; from the accuracy of these results, we deduce the validity of the models used for the lattice simulations. We find that our models provide a satisfactory description for Al^{3+} but are a less precise representation of crystals containing Fe^{3+}; the models used, however, bracket a reasonable range of solute behavior and important trends are unaffected by reasonable changes in the interionic potentials. The simplest vacancy-solute dimer can have either a <100> or <110> orientation; the two constituent defects are closest when the dimer has a <110> axis, but the <100> dimer is more stable because of the large displacement and polarization of the oxygen ion between the trivalent ion and vacancy. Trimers with either orientation are about twice as stable as the corresponding dimers. Complex aggregates of solutes and vacancies, which adopt configurations that form nuclei of the mixed-oxide spinel structure, are even more stable and the stability increases with cluster size. Thus we conclude that such clustering is an important phenomenon at low homologous temperatures. Calculated interstitial formation energies in MgO are large (>10 eV) and our results for the activation energies for solute motion are of the order of 2 eV.

The major difficulty associated with the meaningful calculation of the energies of interaction between ionic solutes and the MgO host lattice is clearly the proper choice of the solute-oxygen repulsive potential. Unlike the case of a pure crystal, reliable repulsive parameters for a solute cannot be obtained directly, and our assumption has been that the parameters are the same as those of the pure solute compound, if these are known. In the absence of such information one must resort to either ad hoc scaling procedures or the direct calculation of Born-Mayer parameters from a consideration of the interactions between free ions. The latter, particularly Hartree-Fock calculations, may yield poor results.

The assessment of the validity of an impurity potential must depend upon comparison with either potentials of known reliability for similar ions or with experimentally characterized impurity behavior. Thus, on the basis of comparison with the Mg^{2+}-O^{2-} interactions and the experimental heat of solution of alumina in magnesia, it seems that the choice of Born-Mayer

terms used here for the Al^{3+}-O^{2-} interaction is a reasonable one, and some confidence may be placed in the results of these calculations insofar as they apply quantitatively to the behavior of the aluminum ion in solution in MgO. In contrast, the calculated heat of solution for Fe^{3+} indicates that the repulsive potential used is too weak. However, relatively minor changes in the substitutional energy would be required to correct this, so that the potential is not grossly deficient. Although the repulsive parameters used here are not correct for a quantitative description of the behavior of Fe^{3+} and Fe^{2+} in MgO, together with those of Al^{3+} they are representative of a range of behavior characteristics of impurities whose interactions with the host lattice may be described as ionic. Within this range, the trends observed in the relative stability of the various defect associates are independent of the variations in the impurity-oxygen repulsive potential, so that improvements in the description of the impurity ion are unlikely (within the framework of HADES) to alter the qualitative conclusions of this work.

The calculated energies are, of course, subject to uncertainty, and it is difficult to make meaningful error estimates. However, the relative energies do not vary radically, changing by about 20% with a substantial change in the repulsive potential. This variation is probably representative. The absolute energies are least reliable, but they are also less important as far as the present work is concerned.

Taken as a whole, then, this work leads to several conclusions concerning the interactions among point defects in MgO.

(1) Impurity-vacancy dimers and trimers are energetically stable, trimers more so than dimers. Of the two possible dimer orientations in the MgO lattice, the <100> orientation is more stable by 0.2 to 0.4 eV due to the large displacement and polarization of the central oxygen ion. This result is the opposite of that expected on the basis of a simple monopole interaction between the defects. The neutral linear <100> trimer is likewise more stable than its <110> counterpart by 0.4 to 0.8 eV. The binding energies and the displacement fields show that the linear trimers are essentially two dimers end-to-end, sharing a common vacancy.

(2) Complex associates of impurities and vacancies, based on a "spinel-like" unit consisting of a cation interstitial tetrahedrally co-ordinated by anions and cation vacancies, are energetically more stable than simple dimers, trimers and isolated defects, becoming increasingly so as the size of the cluster increases. The large binding energy of these groupings relative to the simpler dimers and trimers indicates that clustering should be an important phenomenon at low homologous temperatures.

(3) Interstitial formation energies in MgO are large (>10 eV) but are substantially reduced by the presence of adjacent cation vacancies, as occurs in cluster formation.

(4) Activation energies of motion for impurities are of the order of 2 eV.

To the extent that these results are consistent with the existence of a variety of impurity-vacancy associates, they are in agreement with the bulk of experimental data. The greater stability of the <100> dimer/trimer orientation relative to its <110> counterpart is in accord with the universal observation that centers having <100> symmetry are more prevalent than those with <110> symmetry, although unknown entropy terms may also be important in this regard. Quantitative comparison is practically impossible because of the lack of a firm body of experimental data. The single study available which addresses itself to the problem of determining the dimer/trimer binding energies interprets the greater concentration of <100> orientation defects in terms of a large entropy term, but the evidence supporting this conclusion is rather weak. The energies calculated provide a self-consistent set of values which clearly indicate a hierarchy of defect structures and which permit a realistic comparison with experiment.

3.6 The Defect Structure of MgO Containing Trivalent Cation Solutes: The Oxidation-Reduction Behavior of Iron

Personnel: W.H. Gourdin, W.D. Kingery and J. Driear

Association energies for ferric ion magnesium vacancy dimers and trimers derived from shell-model calculations are combined with oxidation-reduction equilibria data in concentrated crystalline solutions to derive equilibrium defect concentrations for relatively dilute solutions. The several simultaneous non-linear equations required are solved with a numerical iteration method. Calculated results are compared with experimental determinations of solute concentration and oxygen pressure. It is found that with a slight reduction of the shell-model energies, the defect model is in good accord with experimental data at temperatures greater than 1300°C. At lower temperatures, agreement is poor and it is surmised that solute-vacancy clusters may be important.

The experimental results of this study are in good accord with predictions based on a simple defect chemical model for the behavior of iron solutes in magnesia. The quantitative agreement between calculated and measured values of the ratio $R = [Fe^{3+}]/[Fe]_T$ as a function of the total iron content ($[Fe]_T$), oxygen partial pressure (P_{O_2}) and temperature (T) (for

$T \geq 1300°C$) show that such models, predicated on mass-action relationships between various solute-vacancy associates, are capable of adequately describing the system behavior over a range of several orders of magnitude in partial pressure and total iron content at moderately high temperatures. While it is clear that a spectrum of association and disassociation occurs as the conditions of $[Fe]_T$, P_{O_2} and T are changed, it cannot be inferred from the behavior of R alone that those structures chosen are necessarily the correct ones. It is not possible, for example, to determine from the present data which trimer configuration dominates the defect structure at high iron contents and low temperatures or even if they exist at all in the form proposed. However, these results in conjunction with the shell model calculations indicate that the model tested is highly plausible. Its success in describing the oxidation-reduction of iron indicates that it closely approximates the actual defect structure and that the calculated energies for the various vacancy solute associates are reasonable.

In contrast, the poor agreement of experiment with calculations at 1200°C indicates that processes other than those specifically considered may become important at lower temperatures. Further study of the kinetics of the oxidation-reduction process and the detection of polyatomic defect clusters seems to be indicated.

The conclusions drawn from this work may be briefly summarized as follows.

(1) The optical absorption at 4.3 eV (2880 Å) in the near ultraviolet provides a viable technique for determining the concentration of ferric ions present in solid solution in single-crystal MgO. A calibration curve may be established for specimens heat-treated in oxygen at 1400°C for which $R_O = [Fe^{3+}]_O/[Fe]_T$ is approximately constant at 0.80±0.01. Values for R determined with such a curve are found to be in good accord with previous work.

(2) A defect model consisting of trimer and dimer associates and characterized by mass-action equilibrium constants provides a satisfactory quantitative description of the behavior of $R = [Fe^{3+}]/[Fe]_T$ as a function of $[Fe]_T$, P_{O_2} and T for $T \geq 1300°C$.

(3) At temperatures of 1200°C or less, other defect-solute interactions not considered in the analysis may become important, effectively changing the amount of Fe^{3+} detected optically.

(4) The shell model association energies calculated as reported in the previous section for $Fe_{Mg}^{\bullet}$ and V_{Mg}'' in MgO give a reasonable fit to experimental data when they are reduced by about 20%. This is in accord with prior comparisons with the experimental heat of solution.

(5) The use of numerical methods allows the complete calculation of the defect population implied by a set of equilibrium interactions and the requirements of mass, site and charge balance. This population differs from that estimated on the basis of simple assumptions.

3.7 Shell Model Calculation of the Defect Energetics in MgO

Personnel: S.T. Wu and W.D. Kingery

A) Bulk Energetics

At present our understanding of defect interaction and defect motion in MgO is still at a primitive level. Widely different interpretations are provided for the similar sets of data of diffusion coefficients. As a result, very different values of activation energies are given by different investigators. To gain better understanding of defect motion and interaction in MgO we have calculated both motion and interaction energies of 14 cation impurities: Ca^{2+}, Sr^{2+}, Ba^{2+}, Cd^{2+}, Fe^{2+}, Co^{2+}, Ni^{2+}, Mn^{2+}, Fe^{3+}, Co^{3+}, Ni^{3+}, Mn^{3+}, Sc^{3+} and Al^{3+}. In all, more than 130 values of energies have been calculated. Half of these are the binding energies of a cation vacancy located in the first, second, third and fourth neighboring coordination shell of a cation impurity. Another half are the activation energies of a cation vacancy jump from the nearest neighbor site of a cation ion impurity to another nearest neighbor site and to second, third and fourth neighboring sites. In addition, the substitutional energies have been calculated. These energies could be used to calculate the diffusion coefficients of these impurities with the aid of the method of Manning. However, it is found that even the most sophisticated five-frequency model does not seem adequate for this purpose because we have found that both the nearest neighbor and the second-nearest neighbor can be important in vacancy-impurity binding. The five-frequency model is currently being extended so that our calculation can make direct contact with the experimental data of diffusion coefficients.

Our preliminary value of activation of diffusion for Ni^{2+} at 2.06 eV compares very well with the best experimental result of 2.10 eV. This is encouraging because among all the measured diffusion coefficients of impurities, those of Ni^{2+} are the most reliable. Different investigators using different techniques agreed with each other. Thus the shell model which we use for calculation seems to be supported. Our calculation is made possible by the availability of the efficient HADES (Harwell Automatic Defect Evaluation System) computer program. If the success of our calculation is further consolidated, the shell model as implemented in HADES would be

established as a valuable tool for modeling defect kinetics in oxide ceramics.

B) Formation Energies of Vacancies and Substitutional Energies of Cation Impurities on the Surface of MgO

In coordination with the experimental thrust in the study of grain boundary segregation in MgO we are calculating some of the energies which determine the space charge and impurity distribution in the vicinity of a free 100 surface. Five energies have been calculated. One of them is the energy needed to take a Mg^{2+} ion from the surface to the infinity in a vacuum. The others are the substitution energies of Sc^{3+}, Ca^{2+}, Fe^{3+} and Al^{3+} on the surface. Calculation of the formation energy of an anion vacancy on the surface is underway. With these energies at hand, a calculation of the impurity concentration profile can be attempted.

C) Activation Energy of Divacancy Jump In MgO

As a contribution toward understanding the anion diffusion constant in MgO the activation energy of a divacancy jump has been calculated. The calculated results are 3.57 eV for the O^{2-} jump and 3.65 eV for the Mg^{2+} jump. These values coupled with a fairly high formation energy make it unlikely that divacancies play a significant role in defect kinetics of MgO.

3.8 Defect Interactions and Association in MgO at Low Temperatures

Personnel: T.A. Yager and W.D. Kingery

A CO_2 laser-heated sample EPR spectrometer has been developed to study thermodynamic and kinetic reactions in MgO containing 50 to 4300 ppm Fe at temperatures up to 1200°C. The block diagram of this device is shown in Figure 1. The variation of peak intensities was measured as a function of temperature for the spectral peaks attributed to an isolated Fe^{3+} in an octahedral site and Fe^{3+}-V associates in the 110 and 100 directions, as studied by Low (N.Y. Acad. Sci. 72 [2], 71 [1958]) and Henderson et al. (J. Phys. C.: Solid St. Phys. 4, 107 [1971]). Applying thermodynamic equilibrium relations, it was determined that

$$Fe^{\cdot}_{Mg} + V''_{Mg} = (Fe\text{-}V)'_{110}$$

has an association energy of .82±.3 eV. This is in excellent agreement with the calculated value of .85 eV obtained by Gourdin and Kingery (J. Mat. Sci., in press). The iron-vacancy associates in the 100 direction were more difficult to analyze, but evidence has been obtained indicating that this

Figure 1
HIGH TEMPERATURE EPR APARATUS

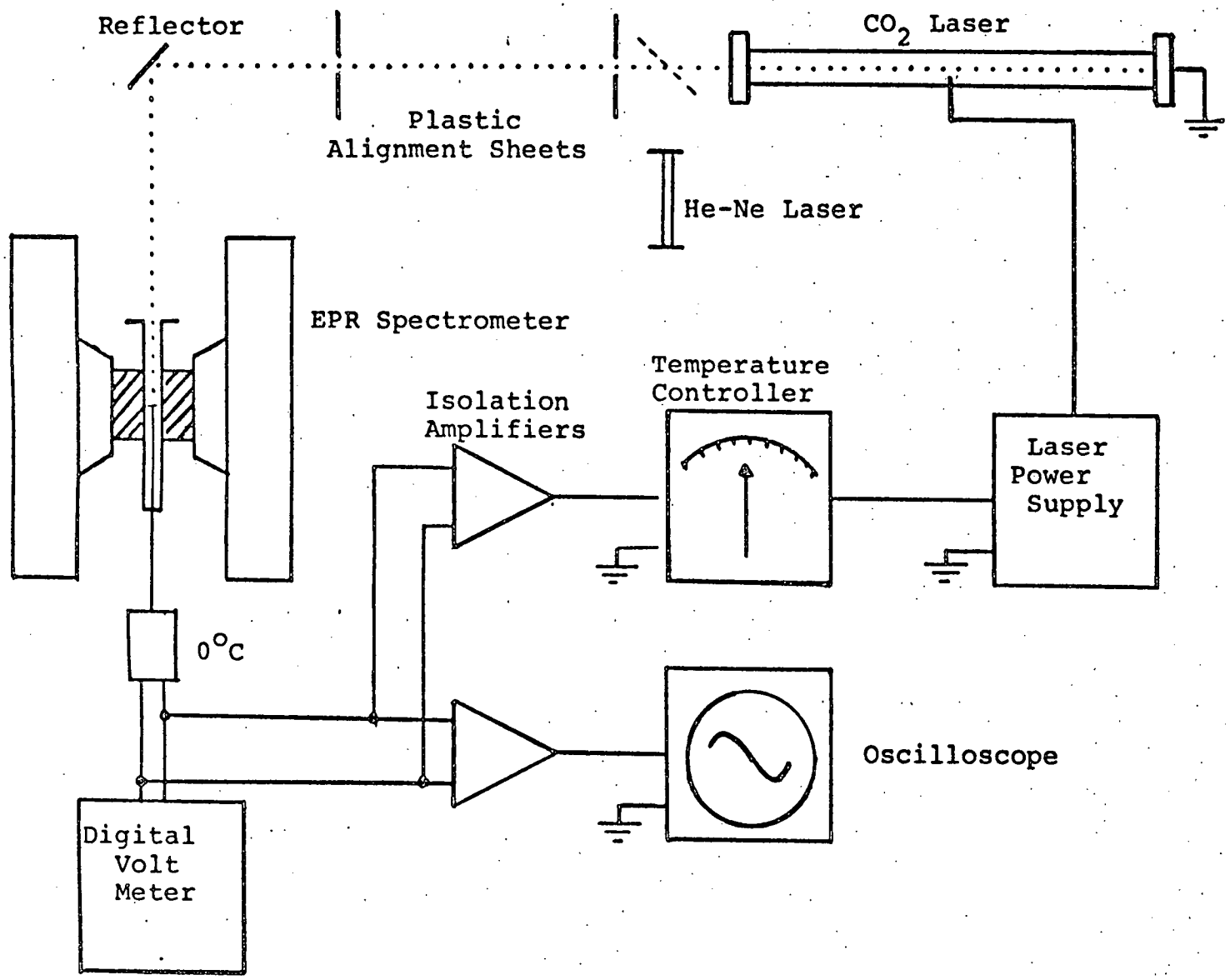

species may be a trimer (two irons associated with a vacancy).

The high-temperature EPR was also used to analyze kinetic relaxation processes. Samples were heated to 1100°C and quenched in the spectrometer using liquid nitrogen. The samples were then isothermally annealed at 400° to 600°C while the intensities of the peaks were measured as a function of time. Below 550°C the associate peaks followed a second order kinetic decay to form clusters or precipitates, with an activation energy of 1.43 eV. At 600°C and above associate peaks first increased in intensity followed by a decay, while the intensity of the isolated iron peak continually decayed. It was concluded that below 550°C the reaction is dominated by the clustering of iron-vacancy associates and above 550°C the reaction is dominated by the association of isolated iron and the vacancy. Using the vacancy diffusion coefficient obtained by Sempolinski (private communication) the low-temperature diffusion coefficient for the dimer (iron-vacancy associate) was approximated:

$$D_{(Fe\text{-}V)'} = 5 \times 10^{-3} \exp\left(\frac{-1.43\ eV}{kT}\right)\ cm^2/sec.$$

Etching studies of MgO samples containing iron were used to study the precipitation reaction. Precipitation was found to be extremely slow in quenched samples isothermally annealed at 500°C, while precipitation was rapid when isothermally annealed at 600°C. It is believed that at 500°C the precipitation reaction is rate-limited by the mobility of the vacancy away from the precipitate and the formation of charged mobile dimers. At 600°C charged dimers are able to form rapidly in the bulk which migrate to the precipitate and vacancies can more rapidly migrate away from the growing precipitate.

A broad peak in the EPR spectra of MgO containing Fe was attributed to ferromagnetic resonance of spinel-like precipitates larger than 25 Å in diameter. This technique is therefore very sensitive to the presence of second-phase precipitates. By isothermally annealing samples and quenching them into liquid nitrogen, the temperature of phase separation was determined for three samples containing different concentrations of iron. These samples are presently being analyzed by quantitative absorption spectroscopy to determine the precise iron concentration.

Future experiments will involve a more in-depth study of the unusual kinetics observed between 500° and 600°C. Additional studies will be conducted using the high-temperature EPR, a superconducting magnet vibrating sample magnetometer, transmission electron microscopy, and etching studies. A correlation between the MgO:Fe system and the MgO:Cr stystem will also be attempted.

3.9 Characterization of Grain Boundary Segregation in MgO by STEM and Auger Spectroscopy

Personnel: Y. Chiang, A.F. Henriksen and W.D. Kingery

Previous studies with STEM, Auger spectroscopy and ion micromilling mass spectrometry have found segregation of solutes such as iron, scandium, calcium and chromium to grain boundaries and surfaces in MgO corresponding to a space charge layer. Most recently, a STEM study has more precisely determined that iron segregates to within about 50 Å of the grain boundary.

In the present study, polycrystalline samples for STEM and Auger have been prepared of MgO with additions of scandium (3000 ppm), iron (550 and 990 ppm), calcium (430 and 750 ppm) and dysprosium (630 ppm). Simultaneous ion sputtering and Auger analysis performed on polished specimens heat treated and air quenched from 1200°C have indicated Ca segregation within a few atomic layers of the surface and Sc segregation within about 30 Å. Similar analyses will be done on the grain boundaries, grain interiors and interior surfaces of polycrystalline samples fractured in ultra-high vacuum and on surface-segregated single crystals with added scandium. With these results and those from X-ray microanalysis of the same polycrystalline samples on STEM, we shall attempt to characterize further the extent and configuration of solutes segregated at grain boundaries and surfaces in MgO.

Uniformly doped powders for the polycrystalline samples were prepared by coprecipitation methods. Hydroxide coprecipitation from aqueous nitrate solution in a back-flow reaction was used to produce magnesium hydroxide plus the hydroxides of Sc, Fe and Dy respectively. An oxalate-hydroxide coprecipitation was used to produce magnesium hydroxide plus calcium hydroxide. Calcination of the hydroxide powders at 900°C for 2 hr yielded submicron particle size materials. Solute concentrations were determined by spark emission spectroscopy (Fe, Ca and Dy) and atomic absorption analysis (Sc).

The six powders were then used to form isostatically pressed rods and hydraulically pressed pellets. These were heat treated in air, first at 1600°C for 4 hr to ensure solid solution, then at 1200°C for one week to segregate the solutes at grain boundaries, and air quenched by withdrawal from the furnace at an initial cooling rate of about 10°C/sec. Surface segregated samples were produced from sections cut from the rods and polished, then heat treated again at 1200°C for one week and air quenched to segregate the solutes at the polished faces. SEM observations of

microstructure were performed on polished and etched samples. In addition, a rod specimen of each composition was notched, chilled to liquid nitrogen temperature, and fractured. SEM observation of the fracture faces showed existence of both inter- and trans-granular fracture in each case.

STEM samples were then prepared from each composition. Small slices were mechanically polished to a thickness of about 2 microns, then ion thinned to perforation with Ar^+ ions accelerated through a potential of 6 kV. A carbon layer of about 100 Å thickness was evaporated onto the specimens to ensure conductivity in the electron beam.

Single-crystal specimens with added scandium were prepared from high purity MgO supplied by ORNL. Thin crystals were isostatically pressed in scandia powder and heat treated, first at 1500°C to diffuse in a calculated amount of scandium and then, with the sintered scandia powder removed, at 1750°C for an extended period to homogenize the specimen. The crystals were cleaved to expose fresh surfaces and heat treated at 1100°, 1300° and 1500°C respectively, followed by an air quench to segregate scandium to the surface.

Two additional single-crystal calibration samples were prepared to establish experimental parameters for quantification of Auger spectra. Although the magnitude of the Auger signal, recorded as peak to peak heights of the dN(E)/dE spectrum, may be said to be proportional to the number of atoms in the volume of analysis, there are a number of contributing factors which must be taken into account. The volume of irradiation is dependent on the size, energy and incident angle of the primary beam, and the actual escape depth of Auger electrons is a function of Auger electron energy, sample lattice geometry and composition, surface roughness, and primary beam angle. The instrument transmission is an additional factor, and in the case of Auger spectroscopy performed simultaneously with ion sputtering, the rate of removal and any preferential sputtering of elements must be taken into account if an accurate depth profile of concentration is to be obtained. In light of these parameters, it can be expedient when accurate quantitative analysis is desired to use a standard of well defined concentration close to that of the specimens, analyzed under identical experimental conditions, to get a direct measure of the absolute peak heights of elements. From this the concentration in the specimens can be empirically determined. Sputtering rates may be determined by interferometry on sputtered areas of a polished, flat sample.

The calibration standard was prepared from high purity MgO supplied by ORNL. A single crystal was doped with nominally 1% Sc through isostatic pressing in scandia powder and heat treatment first at 1750°C to diffuse in

the calculated amount of Sc, followed by an extended heat treatment, with the scandia removed, at the same temperature to homogenize. The crystal was then heat treated at 900°C to precipitate out a scandia second phase. Following SEM observations, a uniformly doped segment was cleaved and re-homogenized at 1750°C. The concentration will be determined by atomic absorption analysis and Debye-Scherrer measurement of the lattice parameter, where concentration can be determined by the empirical Vegard's Law. This calibration crystal will be fractured in vacuum to minimize adsorption and changes in surface chemistry, and ion sputtering Auger analysis will be performed. The second crystal, a sputtering rate sample, was prepared from Norton MgO. It was polished to a flat surface with 20 μ SiC and 5 μ garnet, followed by a final polishing with 1 μ diamond. Optical interference measurements will be done before and after sputtering on a Bausch and Lomb interference microscope to determine depth in the region of uniform sputtering.

Characterization of grain boundary and surface segregation in these samples may be followed by further experiments with the effect of various quenching and cooling rates. Theoretical segregation profiles will be calculated and compared with experimental results.

3.10 Diffusion in Silicon Carbide

Personnel: Y. Tajima, K. Kijima and W.D. Kingery

An understanding of diffusion is important in order to understand and control the processing and properties of ceramic materials. SiC has become of considerable interest in several areas of science and technology and thus it is worth reviewing diffusion studies in SiC. Accurate diffusion data for SiC are difficult to obtain since measurements must be carried out at a high temperature and since high purity material has been difficult to obtain. Also, the interpretation of data is complicated by the covalent and semiconducting nature of SiC.

There have been many diffusion studies of SiC, including both self-diffusion and impurity diffusion. One notable characteristic of diffusion in SiC is the high activation energy (5-10 eV) and a high pre-exponential term (up to 10^8 cm^2/sec). Studies of self-diffusion in pure and doped SiC (n-type or p-type) have shown that the diffusivities of carbon and silicon are dependent on the type of dopant present; for example, carbon diffusion is enhanced by the presence of an acceptor. Similar dependence has been observed for some impurity diffusion. These results, along with the high activation energy, suggest that carbon, silicon and impurities diffuse via

a vacancy mechanism (assuming carbon and silicon vacancies act as donor and acceptor, respectively).

Recent measurements of self-diffusion (Davis, Hon and Hong, to be published) have shown that silicon is the slower moving species in very pure SiC. However, other silicon self-diffusion data (Ghoshtagore and Coble, Phys. Rev. 143, 623 [1966]) showed that silicon is the faster species in Al-doped SiC; the difference between these two sets of data is about three orders of magnitude. This anomaly suggests that silicon diffusivity might be susceptible to sample purity and other experimental conditions. On the other hand, the carbon lattice diffusion coefficients given in both studies agree by an order of magnitude. Carbon grain boundary diffusion as reported in previous studies is several orders of magnitude faster than carbon lattice diffusion. From these results it might be hypothesized that silicon diffusion is more important in diffusion-controlled processes such as sintering and creep and that it may be related to the stoichiometry of SiC.

3.11 Phase Equilibria in Silicon Carbide

Personnel: K. Kijima and W.D. Kingery

It is generally believed that the only condensed phases which occur in the silicon-carbide binary system are silicon, silicon carbide, and graphite. Silicon carbide does not melt at a pressure of 1 atm and decomposes at about 3245°K for α-SiC and 3259°K for β-SiC. Major vapor species under these conditions are C_2Si, Si, CSi_2 and Si_2. Thus a simple reaction equation such as Si + C <=> SiC is inadequate for considering a detailed reaction mechanism. Scace (Proceedings of the Conference on SiC - 1959, Pergamon Press, New York, 1960) found that at high argon pressures and high temperature there is a peritectic point at 3103±40°K in silicon carbide, and the carbon content of the silicon melt is 19 atomic percent. The solubility of carbon in liquid silicon at the silicon melting point is 5×10^{-3} atomic percent. Figure 1 shows the most typical phase diagram of the binary system Si-C.

Silicon carbide is a typical crystal for the study of crystallographic polytypes, which are casued by atomic stacking differences in the direction of the crystallographic c axis. Knippenberg (Philips Res. Rept. 18 [3], 161 [1963]) studied the thermal stability of each polytype from crystal growth data. The stability of SiC polytypes is much affected by impurities such as N, B and Al.

There is much uncertainty with regard to the mutual solid solubilities of carbon and silicon carbide, and silicon and silicon carbide. These solid

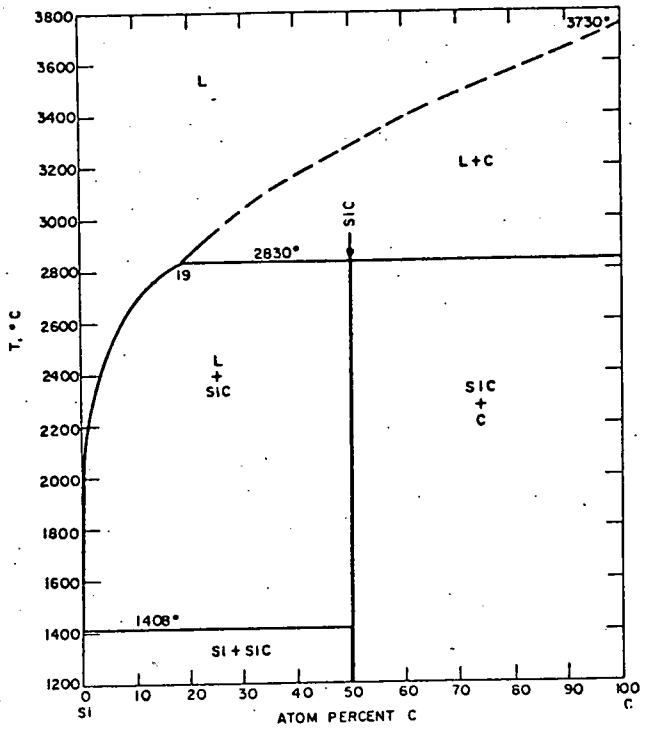

Figure 1. Phase diagram of the binary system Si-C (after R.I. Scace).

solubilities are evidently too small to be measured by chemical means and quantitative data on the existing region of SiC have not been reported. According to Lely (Ber. Dtsch. Keram. Ges. 32, 229 [1955]), silicon carbide is stoichiometric; if there is any deviation of stoichiometry it should be less than 10^{-5} atomic percent. Shaffer (Mat. Res. Bull. 4, 213 [1969]) analyzed the Si:C ratio and found 1.049 for β-SiC and 1.032 for α-SiC, mentioning that although the statistical significance of these values might be questioned, the implication was clear. It has been suggested that SiC at high temperatures may have a silicon-excess structure.

3.12 Grain Boundary Segregation in Silicon Carbide Investigated by STEM

Personnel: Y. Tajima and W.D. Kingery

Grain boundaries and boundary regions are important in all polycrystalline solids. Boron is an important additive in SiC as a sintering aid, but the mechanism of its effect is not as yet clear. One conjecture is that boron segregates to grain boundaries and affects the kinetics and/or thermodynamics. Because of boron's important role in polycrystalline SiC, we have chosen it as the first solute to be studied in the investigation of segregation phenomena in SiC.

STEM has been chosen as an analytical technique since it has a good spatial resolution (∿25 Å) and relatively good sensitivity (∿10^{-19} g) when used in conjunction with energy dispersive X-ray spectroscopy (EDX). This technique has been limited to the detection of elements of atomic number ≥29, due to fundamental problems with the production, collection and the adsorption of low-energy X-rays. However, with the use of a windowless detector it should be possible to detect light elements such as B, N and O.

Samples, sintered and prepared by CVD, have been supplied by several sources. CVD samples, which are very pure, will be doped with boron by ion implantation. Boron concentration profiles will be analyzed by STEM under various annealing conditions. Initial experiments will concentrate on sample characterization; preliminary measurements will be done using sintered samples.

Of the several segregative forces it is suspected that the important ones in SiC are strain energy and the space charge region. This study should lead to a better picture of segregation phenomena in SiC and a better understanding of ceramic processes and properties in general.

3.13 Surface Segregation in Silicon Carbide

Personnel: K. Kijima and W.D. Kingery

Sintering of silicon carbide is successful when done with small additives of boron and carbon. Prochazka (British Ceramic Research Assoc., Special Ceramics 6, 171 [1975]) explains silicon carbide sintering in terms of the effect of additions on the ratio of grain boundary to surface energy. Boron decreases the grain boundary energy due to selective segregation, while carbon increases surface energy due to deoxidation of the surface and the removal of free silicon.

If a small amount of a low-surface-tension component is added, the additive tends to concentrate in the surface layer so that the surface energy is sharply decreased. Consequently, change of surface energy has a non-linear relation with the additive amount between end members. The study of boron behavior at the surface of silicon carbide could be an interesting first step in research on the sintering of SiC.

Of much interest from the viewpoint of LED applications are luminescences occurring upon doping SiC with acceptors such as Al, Ga, Be, Sc and B. Kholuyanov et al. (Proceedings of the Third Conference on Silicon Carbide - 1973, University of South Carolina Press, Columbia, S.C., 1974) summarized some physicochemical properties (including surface segregation) of these impurities in silicon carbide as shown in Table 1. From the viewpoint of not only an analysis of semiconductor properties but of material transport as well, data on surface segregation phenomena in silicon carbide will be required.

Table 1. Physichochemical Properties of Impurities in SiC.

	Solubility Limit (cm^{-3})	Diffusivity (cm^2/s) at 1700°C	Diffusivity (cm^2/s) at 2300°C	Activation Energy at Low Concentrations (eV)	Surface Solubility (cm^{-3})
Al	10^{21}	8×10^{-15}	1×10^{-11}	0.27	1.5×10^{18}
Ga	3×10^{18}	6×10^{-15}	3×10^{-12}	0.25	5×10^{17}
Be	$(5\text{-}7)\times10^{17}$ (at 1700°C)* $(5\text{-}7)\times10^{19}$ (at 2300°C)	8×10^{-10}	1×10^{-7}	0.43,0.62	$(2\text{-}3)\times10^{18}$ at 2300°C
Sc	3×10^{17}		10^{11}	0.5	
B	3×10^{19} (at 1700°C) 1.5×10^{20} (at 2300°C)	1.5×10^{-12}	5×10^{-10}	0.4	$(2\text{-}6)\times10^{18}$

*With impurities introduced by diffusion.

Auger electron spectroscopy (AES) and secondary ion mass spectroscopy (SIMS) give useful surface data which may be important in the analysis of relative impurity distribution change between the surface and the bulk of SiC. The surface solubility of boron in SiC is reported to be 2×10^{18} cm^{-1}, as shown in Table 1. This value is estimated to be somewhat larger than that of AES sensitivity limitation; the sensitivity of SIMS is much higher.

The result of the study of surface segregation of boron in SiC will help determine whether sintering research should focus on the surface or the bulk of SiC.

3.14 Grain Boundary Segregation of Iron in Polycrystalline MgO Observed by STEM

Personnel: T. Mitamura, E.L. Hall, J.B. Vander Sande and W.D. Kingery

We have previously reported that a dedicated scanning transmission electron microscope is capable of both examining a grain boundary in the presence of precipitates and determining compositional variations in the single-phase region adjacent a boundary, and that this method detected iron segregation at a grain boundary in MgO. In the present study, we have applied that technique to investigate more systematically the segregation of Fe at interior grain boundaries of polycrystalline MgO as it depends on concentration and heat treatment.

Samples of MgO were analyzed which contained Fe and which had been quenched from the final heat treatment temperature. Analysis of the segregation configuration at the boundary was done by carefully orienting the boundary parallel to the incident beam and commencing the profile at 1200 Å from the boundary, using 200 Å steps initially and lowering the step spacing to 50 Å near the boundary. In every case the profile of Fe X-ray intensity across a boundary indicated substantial segregation at the boundary with a relatively symmetric concentration profile and a uniform distribution of Fe in the matrix.

Iron-rich precipitates and second-phase regions were observed in samples containing 2900 and 5360 cation ppm Fe. In samples with 2900 ppm Fe which had been slow-cooled from 1500°C, precipitates tended to form along grain boundaries, although many precipitate-free boundaries were also present. Fe-rich second-phase regions were observed in this sample. Extensive precipitation also occurred in samples with 5360 ppm Fe which had been slow-cooled. In samples with 2900 and 5360 ppm Fe which had been quenched from 1500°C or 1100°C, no grain boundary precipitation was seen,

but second-phase regions with an enhanced iron content were present. Samples containing 2900 and 5360 ppm Fe were also annealed at 700°C and quenched. The 5360 ppm Fe samples showed continuous precipitation along the grain boundaries, while some grain boundary areas free of precipitates could be found in the 2900 ppm Fe samples. This indicates that the samples containing 5360 and 2900 ppm Fe in air at 700°C are in a two-phase region in accord with the Roberts-Merwin phase diagram.

Electron diffraction observation of the orientation of grains was carried out for many of the grains observed. In the polycrystalline samples none of the measurements were carried out on identified low-angle boundaries or special coincidence boundaries and for the limited number of samples examined no relationship between Fe segregation behavior and the orientation of the MgO grains was found.

Ca and Si were present as impurities in the samples measured. Ca was present in amounts of 40 to 60 cation fraction ppm and Si was present in smaller amounts as determined by spectrographic emission analysis. As has previously been reported, both Ca and Si were found to be segregated at the boundary within a distance of about 100 Å from the boundary.

3.15 The Solid Solubility of Sc_2O_3, Al_2O_3, Cr_2O_3, SiO_2 and ZrO_2 in MgO

Personnel: A.F. Henriksen and W.D. Kingery

Only a few metal oxide phase diagrams contain information on the solid solubility of one component in the other. By and large, our knowledge of sub-solidus phase relations is confined to extrapolations from one or two experimentally determined points in the phase diagram and, in most cases, the location of these points is not known with a high degree of accuracy.

Tresvyatsky et al. (Poroshkovaya Metalluriya 1, 29 [1964]) first reported on the solid solubility of Sc_2O_3 in MgO. Lopato et al. (Neorg. Mater. 8, 1264 [1972]) later revised the data and found that a maximum of 0.15 mole fraction Sc_2O_3 was accommodated in the MgO lattice at the eutectic temperature of 2260°C. No tabulated data were published, so the phase diagram is of somewhat limited utility.

Evidence of solid solubility of Al_2O_3 in MgO was first reported by Frenkel' et al. (Dokl. Akad. Nauk. SSSR 130, 1095 [1960]), and later a comprehensive study of the sub-solidus in this system was performed by Alper et al. (J. Amer. Ceram. Soc. 45, 263 [1962]). The maximum solubility was determined to be 0.079 mole fraction Al_2O_3 at the eutectic temperature of 1995°C, and an additional point located at 0.008 mole fraction Al_2O_3 and

1680°C was suggested. Stubican and Roy (J. Phys. Chem. Solids 26, 1293 [1965]) determined a fourth point on the sub-solidus to be at 0.043 mole fraction Al_2O_3 and 1880±15°C.

Frenkel' et al. (op. cit.) also first provided experimental evidence of solid solubility of Cr_2O_3 in MgO. Later, Alper et al. (J. Amer. Ceram. Soc. 47, 30 [1964]) determined four points on the sub-solidus and found the maximum solubility to be 0.19 mole fraction Cr_2O_3 at the eutectic temperature of 2350°C. Two contradictory studies on the solid solubility of SiO_2 in MgO exist. Henney and Jones (Trans. Brit. Ceram. Soc. 68, 201 [1969]) found that forsterite was observed in samples containing as little as 0.0034 mole fraction SiO_2 after a heat treatment at 1750°C in argon or air. In contrast, Schlaudt and Roy (J. Amer. Ceram. Soc. 48, 248 [1965]) reported that 0.11 mole fraction Mg_2SiO_4 (corresponding to 0.09 mole fraction SiO_2) could be accommodated in the MgO at the eutectic temperature of 1860°C.

In the MgO-ZrO_2 system only the Zr-rich part has received any attention with respect to solid solubility and we know of no reports on the solid solubility of ZrO_2 in MgO at elevated temperatures.

The present study was undertaken to provide more accurate data for the sub-solidus in each of these systems. One problem in previous studies has been the difficulty in detecting the emergence or presence of second phase at an early stage. The present study employed a technique of heavily etching a heat treated, polycrystalline sample, such that minute amounts of second phase became detectable using scanning electron microscopy (SEM).

The traditional method of heat treating different compositions at one temperature followed by microscopic examination was not used because of the inherent uncertainty as to whether or not equilibrium had been obtained, an uncertainty which becomes more prevalent at lower temperatures. Instead, a given composition was heated at a high temperature until complete solid solution was established. Samples were then heat treated at successively lower temperatures until second phase was detected by SEM, at which point the phase boundary necessarily had been crossed. In addition, the exsolution process was monitored by measuring the change in lattice parameter using a Debye-Scherrer technique.

We have found that the use of heavy etching of the matrix phase provides an extremely sensitive technique for observing small amounts of a second phase.

In quenching studies the appearance of a second phase might result from its formation during quenching. As a result, a necessary aspect of the technique is to identify a temperature at which the quenching procedure provides a sample free from second phase. In principle, an extremely low

nucleation rate might prevent the appearance of a second phase, but in practice the availability of grain boundaries as heterogeneous precipitation sites avoids this difficulty For $MgO-SiO_2$ and $MgO-ZrO_2$ we were unable to bring a second component into solution in amounts that could be subsequently observed as a precipitate. We might have concluded that the kinetics of the dissolution process are so slow that equilibrium has not been reached. However, in these samples, grain growth had occurred with the grain boundaries migrating through the structure and the second phase particles appearing concentrated on the grain boundaries. That is, the second component has been transported through the MgO matrix by a process of dissolution, reprecipitation or diffusion requiring that phase equilibrium prevail.

It has been reported (J.D. Venables, J. Appl. Phys. 34, 293 [1963]) that precipitates containing zirconium in MgO consist primarily of calcium zirconate. It is difficult to obtain a calcium-free MgO and it may well be that the observed precipitates in our samples consisted of $CaZrO_3$ and that the limit reported here does not correspond to the true binary solubility limit of ZrO_2.

The applicability of the lattice parameter analysis is very dependent on the ability to obtain accurate data. It is also dependent on the magnitude of Δa_o (the difference between the lattice parameter of pure MgO and the lattice parameter of the solid solution) and on the concentrations involved. Thus, it is necessary to obtain a sufficiently large change in lattice parameter for the method to be reliable. It may be noted, also, that the method seems more reliable when the Δa_o for the system is positive. If, however, the data from the lattice parameter measurements conform to the equation $\log \Delta a = [-\Delta H/R]1/T + K$, which assumes that Vegard's Law is valid, it is possible to determine the heat of solution for a given component in another without knowing the actual composition. On the other hand, when the lattice parameter falls, it is still possible to attain a temperature interval within which the exsolution must occur for a given composition using the SEM/etch method.

Results of the experimental measurements are summarized in Table 1. As seen there, the heat of solution of Al_2O_3 is greater than that of Sc_2O_3, which is greater than that of Cr_2O_3. Al_2O_3 has the lowest solubility. In all cases, the stable valence state of +3 requires a solution process in which charge-compensating defects are formed along with the substitutional solid solution. The scandium ion, however, has an ionic radius which is essentially identical with that of a magnesium ion in MgO, while the ionic radii of both aluminum and chromium ions are smaller than that of magnesium, the aluminum being the smallest. It can also be seen that the introduction

Table 1. Summary of Results.

Solute	Temperature Range (°C)	Extent of Solid Solution (mole fraction)	Experimental Heat of Solution (kcal/mole)	Experimental Lattice Parameter Change (Å/mole%)
Al_2O_3	1200-1600	0.0004-0.007	48.6	-0.0051
Cr_2O_3	1200-1600	0.007-0.038	21.8	-0.0020
Sc_2O_3	1270-1600	0.005-0.044	36.8	+0.0054
SiO_2	1850	<0.00034	--	±0
ZrO_2	1885	<0.000075	--	±0

of scandium expands the lattice, whereas aluminum and chromium cause lattice contraction. As Sc^{3+} is equisized with Mg^{2+}, the lattice expansion in this case must be due to the formation of charge-compensating cation vacancies or oxygen interstitials. The incorporation of aluminum and chromium in the MgO also creates charge-compensating defects, but a net lattice contraction results since Cr^{3+} and Al^{3+} are smaller than Mg^{2+}.

3.16 Effects of Strain Energy on Precipitate Morphology in MgO

Personnel: A.F. Henriksen and W.D. Kingery

The four different precipitates considered in this study divide into three groups, depending on their morphology.

$MgFe_2O_4$ forms evenly distributed octahedra with {111} habit planes in samples containing small amounts of iron. At larger iron concentrations (or after longer annealing times) the morphology changes into a dendritic type propagating along <100> in MgO.

The second group comprises $MgCr_2O_4$ and $MgAl_2O_4$. The morphologies of these precipitates appear similar, with plate-like forms along a {100} habit plane.

Sc_2O_3 precipitates have a morphology which is dissimilar to any of the above, save the plate-like structure.

The key to understanding these differences seems to be the magnitude of the disregistry which determines the degree to which coherency is maintained in going from the embryo stage to macroscopic precipitate. The strain energy, by and large, is directly proportional to δ^2 for incoherent precipitates, so a discussion in terms of strain energy is equivalent to considering the effect of the magnitude of the disregistry, at least for cubic materials.

As noted by Nabarro (Proc. Roy. Soc. [London] A175, 519 [1940]), an incoherent precipitate is able to decrease its strain energy substantially by taking the shape of a plate. The disregistry for the precipitates in

MgO containing Cr, Al and Sc is so large that a macroscopic precipitate probably would be incoherent. The observed plate-like precipitates in these systems are thus in accordance with expectations. However, the predominantly {100} orientation of $MgCr_2O_4$ and $MgAl_2O_4$, as opposed to the more random orientation of Sc_2O_3 precipitates, cannot be justified merely by the desire of the system to minimize its overall strain energy. It may be explained by assuming that both $MgCr_2O_4$ and $MgAl_2O_4$ form coherently in the embryo stage, in which case the embryo would orient itself along {100} in order to decrease the nucleation activation energy. The substantial decrease in strain energy which is obtained if the embryo forms coherently instead of incoherently is seen from the difference in strain energy in the calculated values for $MgAl_2O_4$. Once the embryo has formed, its growth is enhanced in the direction that minimizes Y. This would account for the macroscopically observed morphology of both $MgCr_2O_4$ and $MgAl_2O_4$.

The random orientation of the platelets of Sc_2O_3 is expected if scandia, even in the embryo stage, forms incoherently in the MgO lattice. Both the magnitude of the strain energy and the fact that the crystal structure of scandia does not consist of a close-packed oxygen sublattice suggest that the incoherency assumption is valid. The incoherent strain energy is of such a magnitude that the nucleation rate will be faster at sites of disorder, where the strain can be relieved, i.e. at dislocations, slip bands, boundaries, etc. Thus, nucleation will occur preferentially at such sites, but the further growth of the precipitate into the MgO lattice will be accompanied by the incoherent strain energy, which can be lowered by forming plates and leads to the observed structure. The orientation of the precipitate embryo is dictated by the nature of the imperfection on which it nucleates, and the plate-like structure is dictated by the necessity to keep the overall strain energy small. This explanation is substantiated by our observations. The fine-line structure along <110> is probably the result of heterogeneous nucleation on slip bands in the MgO, and the fact that all the larger precipitates also are aligned with <110> further indicates that the initial nucleation takes place on the slip bands.

Finally, the morphology of $MgFe_2O_4$ seems to represent a case in which the very small disregistry allows the precipitate to maintain coherency, even when it grows to macroscopic size. If this is true, then the shape of the precipitate has no influence on the strain energy and the system therefore tends to develop the lowest energy interfaces. In the cubic case the lowest energy interface is {111}, which is the one observed. However, the precipitate will eventually grow to a size at which coherency can no longer be maintained, and when the precipitate breaks away from the matrix

it will grow in a direction that minimizes Y. This is the <100> direction in MgO, and larger precipitates should be expected to propagate in this direction, which is observed.

3.17 Grain Boundary Segregation of Scandium in Polycrystalline MgO

Personnel: N. Mizutani, A.G. Reed and W.D. Kingery

Scandium is a trivalent ion in which substantial amounts of the ion enter solid solutions with magnesium oxide. Samples containing 500, 1000, 2000 and 10,000 ppm scandium were heat treated at temperatures ranging from 1200° to 1600°C at times from 48 hr to seven days, and quenched for boundary segregation measurements using STEM. Samples containing iron and chromium and a sample containing each of the three constituents were also prepared by the same heat treatment at the same time.

Samples were prepared by coprecipitation of the hydroxides during continuous mixing. After digestion, the precipitate was filtered and washed with successive solutions of water and acetone, pure acetone, toluene and then acetone. Afterwards the samples were calcined at 900°C to form the oxide, pressed into pellets, and heat treated. The quenched samples were polished with silicon carbide and aluminum oxide and then ion thinned in preparation for STEM measurements.

Initial results indicate that substantial segregation appears; continuing measurements of the segregation profiles are underway.

4.0 Sintering Studies

4.1 Reactive Sintering

Personnel: R.L. Coble

During this year an extensive but not exhaustive review was conducted of reactive sintering systems. This was stimulated by our past work on CaF_2 with small additions of NaF and of ZnO with Bi_2O_3; we found that very large increases in the sintering rate were brought about at temperatures below the eutectics, and that very complex time dependences were displayed as the second component additions approached homogenization in the single-phase fields. Other experimental work on reactive systems was then reviewed, as well as the modeling that has been done to characterize heterogeneous, solid state reactions.

All of the models that have been developed to describe the sintering or hot pressing processes can be regarded as being phenomenological, and applicable to inert elemental substances. The extension to ceramics, for binary systems, including the multiplicity of transport paths have been generated using ambipolar coupling of the charged species in order to maintain electroneutrality; these models are also phenomenological. Even the models for sintering with a liquid phase may be regarded as being for "inert" systems. Many systems that have been manufactured or studied, however, are chemically reactive and introduce, as a result, additional chemical potential gradients than those which arise from the interfacial energies and curvatures, or from applied pressures. For these chemically reactive systems there are two additional characteristics that must be considered which could alter the behavior normally predicted by the first order sintering modeling. First, there are frequently substantial heat effects associated with chemical reactions and the control of temperature may become a problem in addition to the problem of simply specifying the temperature at which sintering operations are being conducted. For reaction bonded silicon nitride, in which silicon powder compacts are reacted with nitrogen from the gas phase, control of the rate of conversion to silicon nitride is necessary to avoid melting the silicon because of the exothermic heat of reaction. In most reactive systems, however, we presume that the reaction rates are low enough that the attendant heat effects will not be as significant as they are in that case.

The second significant effect arises from the chemical potential gradients that are introduced in reactive systems. For a case in which the overall free energy change for a reaction is relatively low, such as for solid solution formation with a limited amount of second component

incorporation in a primary phase, the free energy change can be an order of magnitude larger than that associated with the surface free energy changes which take place due to surface area changes which comprise the sintering or grain growth processes. Most chemical reactions would give even larger free energy changes than does solid solution formation.

In a number of experiments that have been conducted in the solid state, it has been shown that grain boundaries can be induced to migrate due to chemical interdiffusion and in fact migrate away from their centers of curvature; this is opposite in direction to that expected for surface energy motivated boundary migration. Secondly, it has been inferred from some measurements (e.g., Hillert and Purdy) that the grain boundary diffusion coefficient is substantially larger than the boundary diffusion coefficients observed when the boundaries are not moving. The inferences that may be drawn from discontinuous precipitation processes also give larger boundary diffusivities than those expected under static conditions.

These results have two very important implications with respect to sintering in reactive systems. First, the kinetics of transport due to boundary transport can be significantly enhanced; there have been many systems sintered in the solid state in which minor additions give very large increases in the sintering rates that are not accountable for by either plastic flow or by lattice diffusion processes. These include tungsten with nickel, tungsten with palladium, molybdenum with nickel and palladium, calcium fluoride with sodium fluoride, and zinc oxide with bismuth oxide added as well as many iron carbon alloys. We do not now know positively that enhanced grain boundary diffusivities are the most important change that has occurred in these systems. A second phase as a thin film may provide the excess transport that is responsible for the increased rate of the process. Nevertheless, in the reactive systems there are substantial increases in rates observed above those observed when the same materials are pre-equilibrated by heat treatment prior to powder consolidation and sintering. A specific case for a ceramic system is MgO with incorporated iron oxide. Pre-equilibrated material is relatively inert, whereas the inhomogeneously mixed magnesia and iron oxide powders give rise to significantly enhanced sintering kinetics above those exhibited by MgO or the pre-equilibrated mixture.

The second important effect in chemically reactive systems arises from the induced grain boundary migrations that have been observed in several systems, including iron plus zinc from Hillert and Purdy's work, and recently in copper:gold and silver:gold couples studied by Cahn and Balluffi. The induced boundary migration may be important for increased effective boundary

transport, but also for its potential effect on the stimulation of secondary grain growth. Overall, this effect is expected to be important with respect to the change in morphology of particles and pores away from that normally assumed for inert particle assemblages, as will be illustrated below for a liquid-containing system.

There is still another important implication to be drawn from this effect concerning the influence on the measurement of grain boundary diffusion coefficients in chemically reactive systems. When a dopant is diffused into a matrix material, the ratio of the boundary diffusivity to lattice diffusivity deduced from an analysis based on the assumption that the boundaries do not move would be lower than is in fact the case. Thus, many of the experiments conducted on impurity diffusion to characterize the matrix boundary diffusion could be in error because of inadequate characterization and improper modeling to deduce the diffusivity.

For reactive systems containing liquids there have been several metallographic studies conducted which show interesting effects, and specifically that the modeling normally used from inert systems is inapplicable. Huppmann's work (with others) with tungsten containing nickel at temperatures above the eutectic shows that nucleation of the solid solution containing nickel (0.15% Ni) induces migration of the liquid film away from the interparticle necks at an early state of sintering, in contrast to our expectations and predictions. The boundary moves away from the center of curvature, again illustrating the importance of the chemical driving force to form the solid solution and its superiority over the interface motivated boundary migration process.

In working with a positive temperature coefficient resistor ceramic (barium titanate plus titania plus lanthanium oxide), Hoffman (Karlsruche) found that single crystals of barium titanate embedded in the powder matrix were eroded or etched by the eutectic liquid and that in the region attacked the single crystal was converted to micron-sized barium titanate grains. Similarly, in Gauckler's work on the formation of Sialon by reacting aluminum nitride and silica in order to take advantage of the eutectic between those two end members in a disappearing liquid-phase sintering process, the grain size of the Sialon produced was smaller than the particle sizes of the reactant aluminum nitride in silica particles.

The principal point to be made in all of these cases is that the grain growth phenomena are significantly altered from those that have been typical of unreactive inert systems, and provide what would seem to be significant opportunities for application to ceramic materials in which fine-grain sizes are desired for low-temperature, high-technology applications.

Fundamental studies are needed on reactive systems. It should be obvious that the first important aspect to pursue is of detailed characterization of the microstructure evolution. It is from such studies that the differences in behavior have been revealed; further studies are needed to provide sufficient information to analyze the behaviors displayed.

Reaction Models

The modeling that has been done for chemical reactions takes into account the numerous steps in various reaction paths and of multiple parallel paths for some reactions. Because of the large enthalpy changes that accompany most chemical reactions, heat flow to or from the reactor to the reactant particles is one of the reaction steps, radiation and convection to the sample must be considered in parallel, and heat conduction through the product layer to the reaction interface is in series with those "steps." The surface or interface reaction coefficient is another step in the series, diffusive transport of the reactants through the product layer may occur through the product lattice or at grain boundaries or along the surface if the product is porous. Gas evolution requires permeation of the product and boundary layer as well as mass transport in the surrounding atmosphere to complete the series. All such reaction steps require some geometric form for analysis; the most common form assumed is that the reactant particles are spherical, and that the product layer is defined as a concentric spherical shell.

The best model was developed by Carter; he assumed that the rate of reaction was governed by diffusion through the product layer, used the proper diffusion equation for 3-d radial transport, and took account of the volume increase upon reaction (to form a spinel, for example). It is noteworthy that most reactions studied in ceramics as powder mixtures have been analyzed using Jander's older (and less accurate) model instead. However, both models are for single-sized particles; analysis of size distribution effects showed that significant changes in the time dependence for conversion to the product are predicted. No analysis is valid unless the size distribution is known; for most experimental studies on mixed powder systems the size distributions were not reported. Thus, most of the conclusions drawn from the experimental data reported in the literature must be in error. Frequently only the initial reaction rate is analyzed in accordance with Jander's model. This regime should be controlled by nucleation or the surface reaction rate coefficient and therefore be dependent on the total surface area and not on the transport through a product layer which probably becomes rate controlling at larger degrees of conversion. Additional characterization is generally needed:

What is the initial surface area of the reactants?

What is the size distribution of the reactants?

On which of the components does the product form?

Does the product form a dense coherent layer?

Cracking or spalling is to be expected if the volume change is large. Does this occur, and, if so, when?

Without this information, quantitative analysis of the kinetics is meaningless. These results are particularly important for planning our studies on chemically reactive sintering systems.

There are several general conclusions that can be drawn from the studies on calcination reactions, which are endothermic and require some minimum elevation of the temperature before the salt becomes unstable. At temperatures just above the onset of instability, nucleation and growth are expected to be rate controlling; the rate of decomposition in this regime is low. Typically, these processes increase in rate exponentially with temperature, and at higher temperatures some other process step becomes controlling. In $CaCO_3$, for which the decomposition has been widely studied, heat flow becomes important for the intermediate temperature regime. At higher temperatures, the power function increase in heat transfer rate with temperature requires that gaseous diffusion or mass flow become controlling because of the relatively small temperature dependence of diffusion in gases.

4.2 Critical Review of Initial Stage Sintering Models

Personnel: W.S. Coblenz, R.M. Cannon and R.L. Coble

A critical review has been completed of initial stage sintering models. Evaporation condensation, surface diffusion, grain boundary diffusion and lattice diffusion mechanisms provide a set of well posed mathematical problems. However, the sintering literature contains models which differ from one another by orders of magnitude in the time predicted to reach a given neck size for a given mechanism. For both surface and lattice diffusion models, the range of approximations made by different authors results in orders of magnitude differences in times predicted to reach a given neck size at small neck sizes. The various models are in closest agreement regarding the time to reach the end of initial stage sintering, although differences in predicted neck growth rates are significant at all neck sizes.

We are confident that the models selected for evaporation condensation, surface diffusion, and boundary diffusion are reasonably accurate. The lattice diffusion model is regarded as being the least satisfactory of the set because of the complexities involved in describing the evolution of the

neck geometry and the uncertainty in the flux equations from both the sphere surface and the grain boundary to the neck. The substantial differences in the surface diffusion models indicate the large errors which can arise from improperly treating the problem of undercutting. We suggest that approximations must adequately conserve volume even at the expense of other physically distasteful features such as having discontinuities in driving force. The effects of such shortcomings can be anticipated and approximately compensated. Nevertheless, the flux equation of Wilson and Shewman (Trans. AIME 236, 48-58 [1966]) is arbitrary, and similar plausible estimates by others are as much as a factor of three different for the flux from the sphere surface to the neck. In contrast, we suggest that the errors arising from the geometrical simplifications of Eadie et al. (Acta Met. 22, 1185 [1979]) are less severe and the relations for the mass flow from the boundary are more accurate. Most of the flow is to the near neck region for which the flow path is not much changed in spheres; further, the flux to the far sphere surfaces is probably overestimated by less than a factor of two because of the divergent flow field. The ratio of the fluxes from the sphere surface and grain boundary to the neck by lattice diffusion depends on the details of the neck curvature. Undercutting decreased the neck curvature. The degree of undercutting will depend in detail on the relative magnitude of these two fluxes, and so models which ignore undercutting, or only approximately treat it, as we have done, are quite approximate. We suggest that a proper computer simulation of the lattice diffusion model, including fluxes from both the sphere surface and the grain boundary to the neck, and allowing for the evolution of the neck geometry from both fluxes, would be very useful and probably necessary to resolve this problem.

Experimentally, it is relatively rare that it can be assumed that transport on only one path will be important for the range of neck sizes and temperature of interest. At the boundaries between two fields, in which a mixture of mechanisms must be considered, the improvements in modeling suggested here make combination modeling more difficult. In most previous efforts, simple addition of neck growth rates for each mechanism considered seemed to be a reasonable approach. Although the local fluxes will change in detail, the addition of the separate fluxes using equations from the individual models seems an adequate approximation for most cases. This expectation seems justified by comparison of the rates predicted by adding neck growth rate for each mechanism with the more exact calculations of Eadie et al. for specific ratios of boundary and lattice diffusion. The major problem arises from the different and more complex relations between p and x for the alternative paths. Various weightings of the contributions

to p as a function of x can be envisioned such as were used to arrive at the approximate lattice diffusion model. The p-x relation for a mixed mechanism is estimated by averaging the p-x relation for each mechanism using the neck growth rate for that mechanism as a weighing factor. For example:

$$\overline{p} = \frac{\sum_n p_n \left(\frac{d(x/a)}{dt}\right)_n}{\sum_n \left(\frac{d(x/a)}{dt}\right)_n}$$

where p_n is neck curvature as a function of x for the n^{th} mechanism, and $[d(x/a)/dt]_n$ is neck growth rate for that mechanism.

It would be extremely desirable for more computer calculations to be done such as those of Bross and Exner (Acta Met. 27, 1013-1020 [1979]), who considered both surface and boundary diffusion. These should be presented in a form which allows comparison of the rates using approximate additive relations as well as elaborating the detailed differences and refinements.

The integrated neck growth rate expressions which we have selected following this assessment that describe the initial stage solid state diffusion mechanisms are as follows:

* Evaporation-Condensation $$\left(\frac{x}{a}\right)^3 = \left[\frac{6\alpha\gamma p^\circ \Omega^2}{\sqrt{2\pi m}(RT)^{3/2} a^2}\right] t$$

* Grain Boundary Diffusion $$\left(\frac{x}{a}\right)^6 = \left[\frac{192 D_b W \gamma \Omega}{RTa^4}\right] t$$

* Surface Diffusion $$\left(\frac{x}{a}\right)^6 = \left[\frac{25\delta D_s \gamma \Omega}{RTa^4}\right] t$$

* Lattice Diffusion $$\left[\frac{1.32}{1.32 + (x/a)^{1/6}}\right] \left(\frac{x}{a}\right)^{4.83} = \left[\frac{115.4 D_\ell \gamma \Omega}{RTa^3}\right] t$$

The goal in the selection of accurate models goes beyond the desire for improved mechanism mapping. Accurate models are necessary for adequate experimental confirmation of their validity. If we were confident that the models were accurate and met the assumptions in experimental work (spherical particles of one size) and that the size-temperature space under study was for a single mechanism of transport, the kinetic data from sintering could then be used as a source of diffusion data. However, continued characterization of neck sizes and shapes and shrinkage is regarded as mandatory for any such confidence. The principal point to be made with respect to experimental work is that characterization of the structures is

mandatory if we are to proceed to generate suitable models to reliably predict the kinetics as well as ball-park estimates of the sintering rates. We agree with Johnson that detailed confirmation of models will be much more satisfactory if the evolving geometry is characterized metallographically rather than assumed to conform to a simple approximation; particularly when multiple transport paths are potentially important, measurement of both shrinkage and neck growth is mandatory for satisfactory identification of the controlling model.

4.3 Surface Area Reduction of Alumina Powder Investigated by BET and TEM

Personnel: J.M. Dynys, W.S. Coblenz and R.L. Coble

In the previous report no effect of MgO additions on the surface area reduction kinetics (with and without shrinkage) of Alcoa XA-139 was determined. However, prior to the onset of shrinkage, surface area had decreased from 25% to 40% by rapid heating and cooling from R.T. to 1000°C. It had been asserted then that this effect was due to the elimination of fines. Further characterization of this powder by BET has shown considerable batch-to-batch variability in the surface area per unit weight. Brief TEM studies on the as-received and calcined powder verify qualitatively that fines are eliminated rapidly. In an attempt to quantify this, a particle size distribution on the as-received powder was determined. Estimating the surface area from this distribution gave values slightly less than the BET determined surface area. Using the fine portion of the distribution curve in conjunction with the measured surface area reductions in order to estimate surface diffusivities gave variable results. For instance, at 1000°C, a spread greater than 10^3 in the deduced surface diffusion coefficients was determined because of uncertainties in packing arrangements and uncertainties in the distribution of fines. For this reason the use of surface area reduction kinetics for determining surface diffusivities from commercial grade powders has not been pursued further.

A positive result of the TEM studies, however, is that due to the rapid elimination of fines (leaving a coarse distribution), the previous year's measurements with and without MgO still suggest that magnesia has little effect on the surface area reduction in alumina.

4.4 Initial Stage Sintering Mechanisms and Neck Growth in Sphere-Plate Experiments in Alumina

Personnel: J.M. Dynys, R.L. Coble and R.M. Cannon

Sintering of alumina has been studied for more than 20 years by a host of investigators. The interpretations of these studies have not yielded a common agreement upon the rate-controlling transport path, nor have subsequently estimated mass transport coefficients (for a single mechanism) produced agreement with those deduced from other mass transport studies or independently measured ones. Reasons for this often stem from how and which sintering equation was used and to a greater extent from the complexities of powder compacts that are not considered in those equations. As a result of this, measured parameter dependencies and mass transport data deduced from sintering (particularly from powder compacts) have been regarded as unreliable.

There is an alternative approach that may lead toward a better understanding of sintering, which is to use the model geometry experimentally to confirm expectations based on the best set of model sintering equations used in conjunction with a reliable set of mass transfer coefficients. Varying model parameters in this approach will in principle verify transitions from one rate-controlling path to another. However, predictions fall into two categories based on currently reported δD_b^o values. In creep studies, δD_b^o has been deduced to be relatively rapid from the strain rate: grain size behavior. Proton activation tracer diffusion studies on polycrystalline samples have produced a δD_b^o value with a much lower relative magnitude and an apparently high (>200 kcal/mole°K) activation energy. Use of the latter value for predictions of creep and sintering behavior contradicts previously observed results. Neck growth data support the use of either δD_b^o value assuming that the δD_b^{Al} deduced from creep is not applicable. These results are postulated from magnitude comparisons of deduced and reported diffusivities. In all cases, rapid oxygen transport along the surface was assumed allowing lattice diffusion to contribute to both shrinkage and coarsening.

Model experiments (polished sapphire spheres to a polished sapphire plate) were performed in a vacuum furnace equipped with tantalum heating elements and shields. The spheres were held in a sapphire sandwich affair consisting of a plate-retaining ring-cover plate. This sandwich, in order to reduce vapor effects, was placed over a partially sintered, coarse, high-purity alumina powder held within a covered tungsten or alumina crucible. Doping with magnesium was accomplished by vapor phase equilibration of the

sapphire plates and balls (separated into open Mo boats) over a two-phase mixture of spinel and alumina at the sintering temperature. Neck sizes and shapes were subsequently recorded by first fracturing the spheres from the plate and then photographing the necks found on the plate. Where investigated, the neck patterns on the spheres were noted to be mirror images of those found on the plate.

Several interesting features of the neck growth have been noted. For all sizes, undercutting and neck instability have been found. Undercutting is indicative of either a surface or lattice diffusion mechanism. In general, the larger the sphere the more pronounced was the instability or finger-like growth (this breakup is analogous to a cylindrical instability). Preferred growth directions and faceting are prevalent which reflect the anisotropic nature of WD_s and/or γ_{sv} on alumina surfaces.

Because of the existence of the instability of the neck surface, analysis of the neck growth was conducted using both the maximum and minimum diameters observed for each neck. This range of experimentally observed neck sizes precludes the establishment of an exact size or time dependence from the data analysis. However, the data were plotted in this fashion. The results of the normalized neck size $(\frac{x}{a})$ versus size at a constant time and temperature do not favor any one size exponent. Further, the results indicate that a slope of 1/5 or 1/6 (but not 1/4) can be easily fitted to the time dependence ($\frac{x}{a}$ versus time for each size) of the data. This result supports our current modelling.

The results obtained by comparing the magnitudes of the estimated diffusion coefficients with the accepted lattice and surface values and with the possible boundary diffusion coefficients show the following:

a) Agreement with aluminum lattice diffusion-controlled neck growth was found, but no effect of MgO doping was exhibited.

b) Poor agreement with the aluminum boundary diffusion (based on creep) case.

c) Agreement with surface diffusion-controlled neck growth.

d) Agreement with oxygen boundary diffusion-controlled sintering.

Three possible explanations evolve from the possible diffusion data, observed neck growth data, and powder compact observations.

Case I

δD_b^O is rapid but δD_b^{Al} is less than the creep value. In this case, the observed neck growth should have contributions from both D_L^{Al} and WD_s control. However, the trend is for WD_s to be more important at smaller particle sizes. If this is true, then no initial stage shrinkage should be observed; rather, extensive coarsening would result.

Case II

If δD_b^O (Reddy) is true, then no lattice kinetics and only a small amount of boundary kinetics would be observed for the sphere sizes used here. Again, smaller particle sizes would be expected to coarsen but not shrink.

Case III

Model geometries have problems with special orientations and boundaries that would not be expected in powder compacts. If the tracer δD_b^O were controlling, then Case II again exists for a powder compact. Likewise, Case I is appropriate for a δD_b^{Al} which is less than the creep value. However, if the creep boundary aluminum value is true, then powder compact sintering should be WD_s controlled at low temperatures (<800°C) and boundary limited with significant contributions from surface and lattice diffusion at higher temperatures predicting simultaneous shrinkage and coarsening.

In summary, best experimental fit, judging from the observed neck growth data, its independence of MgO doping, notable undercutting, and neck shape instabilities, suggests that surface diffusion is dominant for the neck growth measured here. Paralleling this conclusion is the assertion that special orientation problems are associated with model experiments, and further, our present understanding of boundary diffusion is inadequate.

4.5 Grain Boundary Grooving and Surface Diffusion in Alumina

Personnel: J.M. Dynys and R.L. Coble

The role of surface diffusion in the sintering of alumina has been speculated upon for a number of years without a conclusive trend prevailing. As a first step in assessing this problem, the currently published values of the surface diffusion coefficients (or product of the surface width and surface diffusivity which will be referred to henceforth as WD_s) have been reviewed. Values which seemed unlikely to have contributions from other transport mechanisms or inadequate sample characterization have been plotted as lines on Figure 1 over the temperature range in which the data were measured. Three sets of values are apparent. In the low temperature regime, two values, deduced from surface area reduction measured by gas permeability on powder compacts, reveal a relatively low activation energy, a wide variation dependent upon powder size and compact density, and a relatively higher magnitude than expected by extrapolation of the bulk of the higher temperature values. Because of the wide variance noted for different size powders, the magnitude of these data at low temperatures have been suspect, but the observed lower activation energies are not easily explained unless a

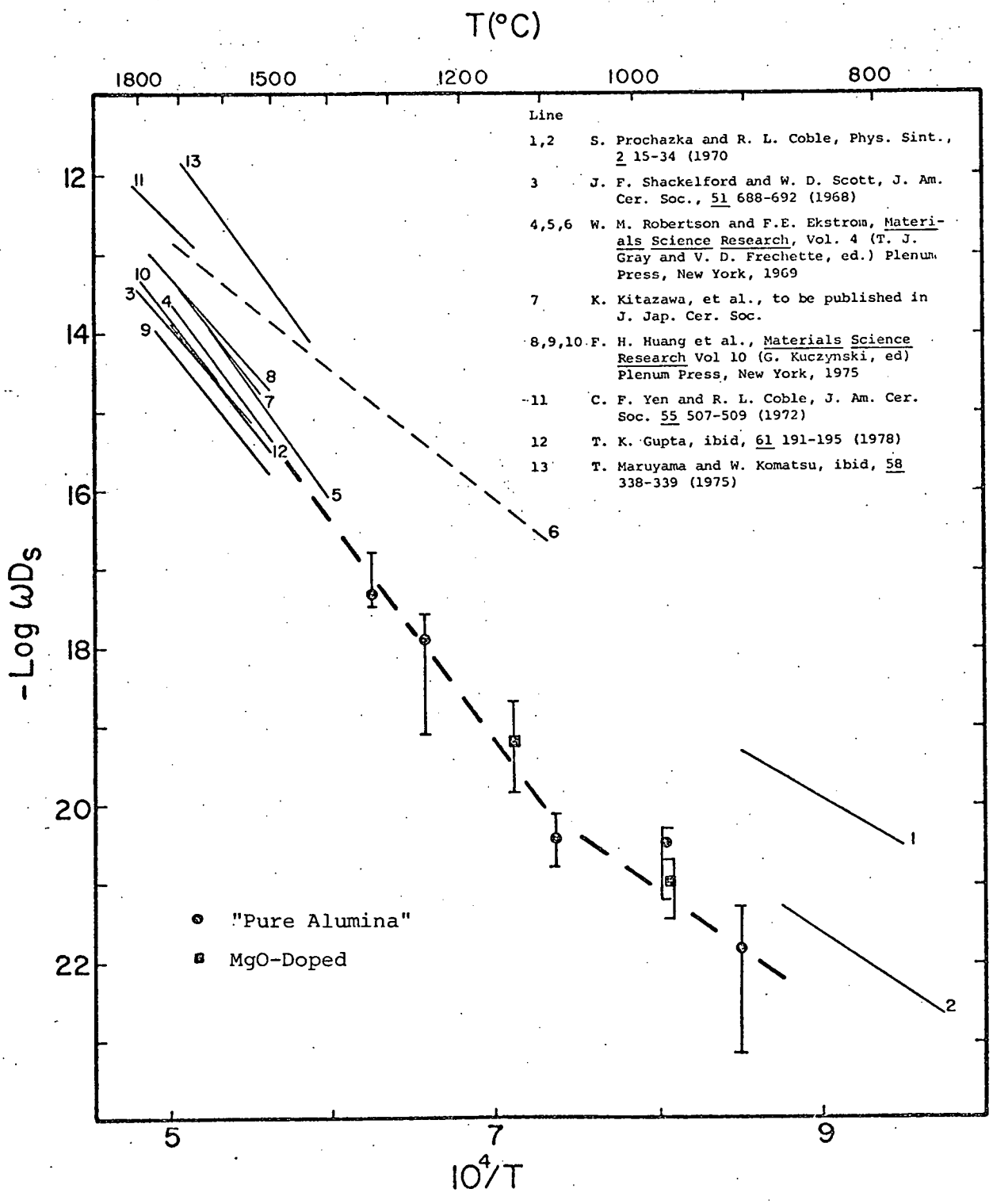

Figure 1. Summary of previous results on surface diffusivities in alumina and our recent results from boundary grooving experiments on undoped (●) and magnesia-doped (■) specimens.

systematic error in the technique exists.

In the high temperature regime, the two sets of reported diffusivities exist (defined by lines 3-10, 12 and lines 6, 11 and 13). These lines were estimated from grain boundary grooving, amplitude decay of gratings of various wavelengths and of a single scratch, and by measurement of the characteristic void spacing formed upon breakup of long, cylindrical pores. The bulk of these values falls within the band between lines 8 and 9. These extremes are the results from amplitude decay studies on (0001) and $11\bar{2}0$) planes on sapphire. An indication of the anisotropic nature of WD_s or of the surface energy (γ) is apparent especially when the faceting and scatter accompanying studies of this type are noted. Volume diffusion contributions to these processes can be shown to be negligible when either ion is presumed to be rate controlling. Grain boundary grooving results on bicrystals (low misorientation angles) by three independent investigators have yielded lines 3, 4 and 10, which are in remarkable agreement with one another (even though contrasting air and vacuum ambients were used). The only polycrystalline material studied, using boundary grooving, was magnesia saturated alumina (Lucalox), represented by line 5. This slight enhancement (compared with 3, 4 and 10) may be a result of some volume diffusion contribution to grooving (D_L^{Al} deduced from creep of magnesia saturated alumina is approximately 10 times D_L^{Al}-tracer in this temperature range), surface diffusion enhancement by MgO additions, or simply experimental scatter often associated with oxides.

Curve 6 was calculated from the grooving results for an impure material that was characterized by the formation of second phases on the surface. It has been included here to suggest the possibility of increased magnitudes for an extracted WD_s where high impurity content is present. The extent to which impurities affect WD_s cannot be ascertained in grooving studies because of the known enhancement of volume diffusion. Using this magnitude and the above agreement, the values of lines 11 and 13 appear to be too large although no apparent reason for this was found.

In order to extend confidence in the available WD_s values to the lower temperature ranges, grain boundary grooving experiments on both very pure and magnesia-saturated (Lucalox) alumina have been conducted. Groove widths have been determined by stereolography and topologic induced contrast effects in the scanning electron microscope. These ranges of WD_s determined from the band of observed widths are also shown in Figure 1. The median value of the observed widths was used to estimate the WD_s value shown by the symbols.

Drawing the best line through the data determined here (weighing the

observed 1086°C value less than the others) produces a line which does not include the band of values discussed above. Weighing these published values accordingly, the heavy dashed line was determined as an adequate fit at temperatures above 1100°C. However, an apparent knee in the curve must then exist in order to include the low temperature data observed.

No large difference in grooving widths for the two types of samples used was observed. However, the degree of faceting found on the Lucalox samples appeared to be greater than that observed for the pure samples. Since it has previously been observed that Mg additions retarded this effect at higher temperatures, further characterization of these samples is planned along with investigations of variable times at each temperature, and of orientation effects to determine whether "special" grain boundaries introduce surface reaction resistance to the D_L-controlled regime.

4.6 Heating Rate Effects in Sintering

Personnel: R.L. Coble, J.E. Blendell and J.M. Dynys

We have been interested in the influence of heating rates and variable heating rates on the evolution of microstructures during sintering because of the fact that we use constant heating rate apparatus in the collection of experimental data on shrinkages and because all commercial operations are conducted at some specified heating rate. In addition, there have been various experiments which show that variable controlled heating rates are necessary, in some cases to avoid cracking, and/or to control drying and binder burnout. Otherwise, there have been experiments which show that rapid heating rates are beneficial in achieving high density in relatively short times. Our analyses have been based on the various mechanisms of material transport by which sintering takes place. We have ignored, at this stage, the important effects related to drying and to binder burnout.

In accordance with our mechanism mapping for aluminum oxide, which gives the conclusion that surface diffusion is the dominant mechanism at low temperatures and that grain boundary diffusion becomes important at higher temperatures, one could automatically assume that a rapid heating rate to a temperature at which grain boundary diffusion is dominant would be beneficial because of a reduction in the contributions from surface diffusion as a coarsening mechanism would be inhibited. Focusing on those two effects alone, we presume that a mixed mechanism mode of densification and coarsening can be prescribed as a function of heating rate by proper integration of the diffusion coefficient: time products over the heating rate and to the peak temperatures of interest. Upon

comparing the models for surface diffusion and grain boundary diffusion for their contributions to neck growth given above, it is noteworthy that they both have the same time dependences and size effects. Consequently it is only with changes in temperature that changes in the relative magnitude in the contributions of these two mechanisms can be displayed or expected. We have used several summation techniques with variable time increments in order to assess the overall integrals for the contributions to neck growth to a given high temperature. The primary problem that arises, or that has existed with respect to the predictions that we might make for the heating rate effects with these two mechanisms, has resulted from our uncertainty concerning the surface diffusion coefficients and their activation energies. The principal data that we have utilized are those from Prochazka, for which there is a relatively large uncertainty in the magnitude of the D_o's and a variability in the activation energy as well.

The results of our studies have led to two conclusions. First, a very high heating rate would be required for sinterable powder (that is, micron-sized powder) in order to reach the regime in which grain boundary diffusion is controlling prior to completion of the initial stage of the process by surface diffusion; heating rates of the order of 10^4°K per second would be required. Secondly, after many calculator runs of the integrations, we have confirmed that an approximation proposed by Cutler some years ago is quite accurate in giving the value of the integral over time, i.e., the integral of D(t)Dt is approximately equal to $D_{max} T^2_{max}$. From these results, we have concluded that a strip heater with very thin specimens would be useful for determining whether the changes in microstructure evolution that are predicted from the modeling do in fact occur.

4.7 Sintering of Covalent Materials

Personnel: W.S. Coblenz, R.L. Coble and R.M. Cannon

Covalently bonded materials, notably SiC and Si_3N_4, are candidate materials for various high-temperature structural applications, having good oxidation resistance, creep resistance, high strength, and thermal shock resistant properties at high temperatures. These materials have been hot-pressed to high density, usually with a liquid phase present, and parts have been machined to shape. Reaction sintered silicon carbide has been commercially available for many years. This material is formed by siliconizing mixtures of carbon and silicon carbide grain. Strength, high-temperature creep and oxidation resistances of the reaction sintered materials are generally inferior to the hot-pressed material. The development of

sintered silicon carbide is notable because it combines the best properties of hot-pressed SiC and the flexibility of using fabrication techniques (i.e., die pressing, ejection, molding, slip casting) to produce near-net shape products, which is the strong point for reaction sintered material.

It is the objective of this study to investigate the sintering mechanisms important in covalent materials. Silicon has been chosen as a model material for several reasons. Impurity solubilities and their acceptor or donor levels are known for many dopant elements. Diffusion data are available for impurities, self-diffusion mechanisms have been studied to some extent, and silicon is available in high purity.

The two general characteristics of semiconductors which have the greatest consequence for their sintering behavior are intrinsically low self-diffusion coefficients compared to metals and oxides at the same fraction of their melting points, and the tendency of their surfaces to combine with impurities to form a large variety of surface phases. The low self-diffusivities require small particle sizes for reasonable shrinkage rates, but may also promote undesirable and competing coarsening processes. For example, comparing copper and silicon at their melting points, their self-diffusivities and vapor pressures are:

$D^*_{Cu} = 2.1 \times 10^{-8}$ cm^2/sec $\qquad p^\circ_{Cu} = 4.34 \times 10^{-7}$ atm

$D^*_{Si} = 5.17 \times 10^{-12}$ cm^2/sec $\qquad p^\circ_{Si} = 4.9 \times 10^{-7}$ atm

It has been shown (Greskovich et al., J. Am. Ceram. Soc. 59, 7-8 [1976]) that silicon powders exhibit the coarsening versus shrinkage competition typically found for covalently bonded materials, and that boron is an effective sintering additive. The sintering behavior and the results of Auger and LEED studies (J.J. Bellina, Jr., Jap. J. App. Phys. 13 [1974]) both strongly suggest that the role of boron is to segregate to surfaces at the sintering temperature, impede vapor transport, and thus reduce the coarsening, allowing the shrinkage mechanisms to dominate.

A) Measurements on Silicon

Silicon samples have been prepared by arc melting 4-N^+ silicon powder undoped or with 0.2 wt% boron. Auger analysis shows boron surface segregation in the boron-doped samples heat treated at 1300° and 1350°C. Copper-containing precipitates were observed at grain boundaries in SEM examination although present in too small an amount to be observed by Auger. Copper contamination probably results from either the arc melting process or sample polishing. Copper diffuses rapidly in silicon and can precipitate

during quenching, so its effect on the surface properties at high temperature is uncertain.

Evaporation rates of silicon samples have been measured using a step-height technique in which part of a sample being heated is masked off, thus producing a step-height which can be measured with a two-beam interference microscope if the sample does not facet or roughen excessively. It was observed that undoped silicon surfaces, freely evaporated, tend to facet. The boron-doped samples, freely evaporated, develop an undulating surface with a wave length of about 4 microns. Auger analysis indicated higher boron content on the freely evaporated surfaces than on the masked surfaces of the boron-doped samples. Boron enrichment is to be expected because the vapor pressure of silicon is nearly four orders of magnitude greater than boron at the melting point of silicon.

We have qualitatively interpreted the surface structure seen on boron-doped samples to be due to an instability analogous to constitutional supercooling at liquid-solid interfaces. The implication for sintering behavior is that both composition and curvature must be considered in determining the driving force for mass transport.

If the solvent (silicon) is Raultian and the solute (boron) is Henrian, then the vapor pressure of silicon, P_{Si}, is:

$$P_{Si} = P^{\circ}_{Si}(1-X_B)\left(1 + \frac{\gamma\Omega}{RT}k\right)$$

where P°_{Si} is the vapor pressure of pure silicon, X_B is boron concentration, and k is surface curvature. Calculations using the quasi steady-state approximation to link the silicon transport in the vapor phase to the boron transport by lattice diffusion indicate that vapor phase transport can be reduced by a factor of 10^3 for particle sizes of interest in sintering. For an initial stage sintering model with neck growth by vapor transport, the condensation rate at the neck is given by:

$$J_{Si} \approx \frac{\alpha P_{Si}\gamma\Omega}{\sqrt{2\pi m}(RT)^{3/2}\rho} F,$$

and, for $F < 1$,

$$F = \left[\frac{D_B\sqrt{2\pi mRT}}{X_B\rho\alpha P^{\circ}_{Si}}\right].$$

F is the factor by which the condensation rate at neck is reduced beneath that predicted by the use of the Langmuir condensation rate; ρ is the radius of curvature at the neck; D_B is the lattice diffusivity of boron in silicon;

X_B is the atom fraction of boron; and $\alpha \approx 1$ is the Langmuir condensation coefficient.

If the above model is accepted, then the effectiveness of boron as a sintering additive for silicon is due to the (low) lattice diffusivity of B in Si which then controls the vapor transport of silicon. This is an interesting conclusion since coarsening mechanisms are thought to dominate because of intrinsicly low lattice and/or grain boundary diffusivities.

Langmuir evaporation rates measured by both the step-height technique and weight loss measurements indicate a small (factor of 2), if any, effect of boron, and that the Langmuir evaporation coefficient is not greatly different from unity. Weight loss measurements have been carried out in a specially constructed sapphire tube vacuum furnace in order to minimize contamination.

B) Spheridization of Powders

A water-cooled quenching chamber has been built and tested for use with plasma spraying equipment for the spheridization of powders. Spheres $\lesssim$40 microns in diameter appear spherical enough for model initial stage sintering studies. Larger spheres are affected by the increase in volume during solidification of the silicon which results in large protrusions on the surface.

C) Measurements on Silicon Carbide

Silicon carbide surface chemistry has been investigated with the scanning Auger microscope. Surfaces analyzed were heat treated at 2000°C in contact with a matching SiC sample to avoid decomposition of the SiC surface. The sample couple (G.E. boron-doped β-SiC) was wrapped in grafoil and placed in a grafoil envelope with boron powder to control the boron activity. Samples were heat treated in flowing argon in a carbon tube furnace. Boron was not detected on SiC surfaces heat treated without the boron powder, presumably due to a lowering of the boron activity by residual oxygen and/or nitrogen in the furnace. Samples heat treated with a high boron activity had a carbon-rich surface layer with boron-rich islands (B/C $\approx$ 1 in boron-rich areas estimated from elemental sensitivities). The boron-rich areas were $\sim$15 Å thick as determined from sputter depth profiling (Figure 1). The boron distribution observed is consistent with a chemical driving force for segregation at high temperature and surface phase separation during quenching to give the boron-rich surface phases. Samples sintered in-house from alpha silicon carbide abrasive grain show an increase in the boron Auger signal during sputter depth profiling (up to 0.1 μ). This

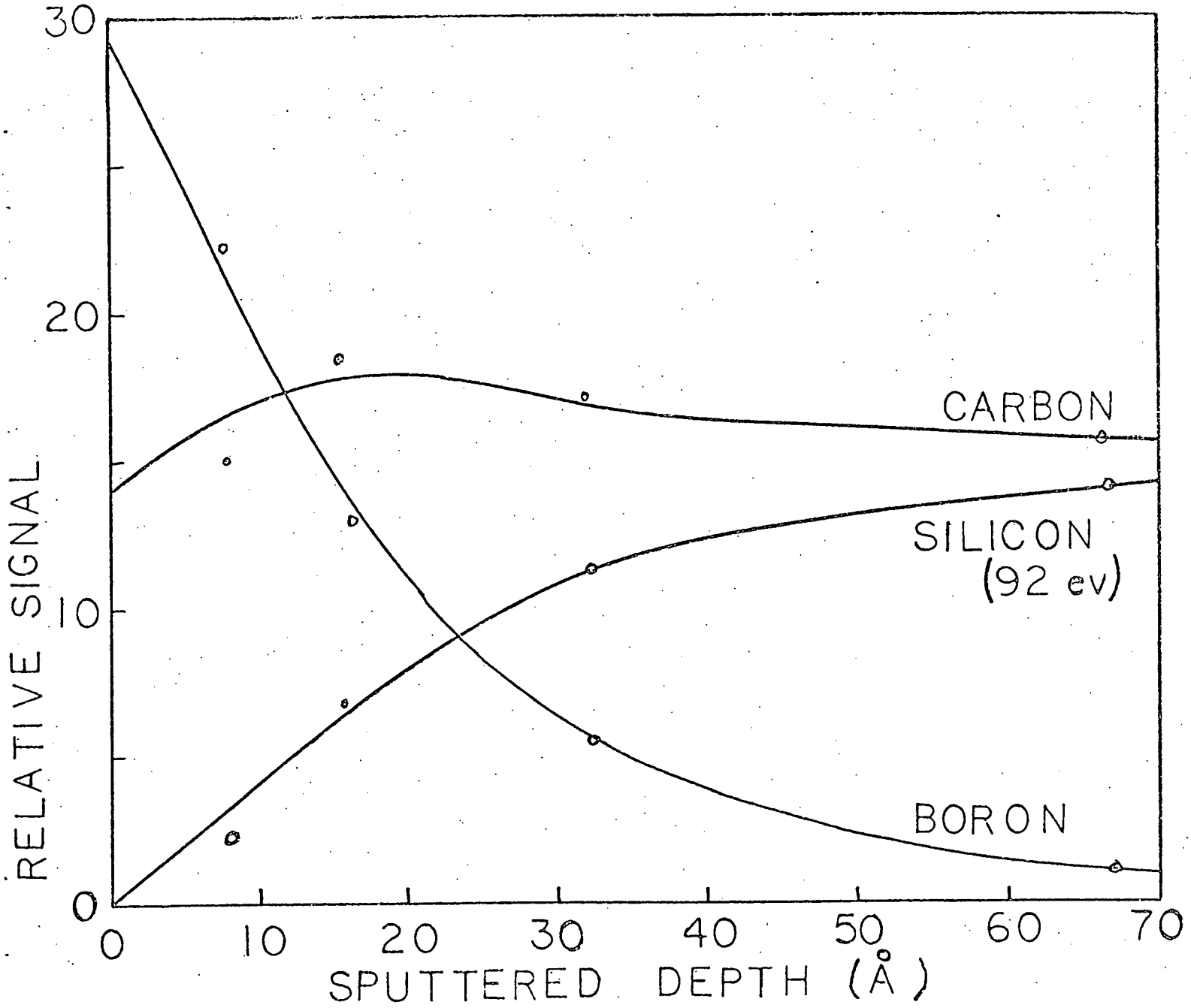

SPUTTERED DEPTH PROFILE
BORON RICH AREA ON SiC

is due to pick up of tungsten during ball milling which reacts with boron to form WB_2. Preferential sputtering of the SiC matrix gives an increase in tungsten and boron signals.

Examination of the in-house α-SiC sintered samples in a STEM (scanning transmission electron microscope) revealed a high density of tungsten-containing precipitates. Grain boundaries in the α-SiC and the G.E.-doped β-SiC show no segregation of heavy metals. Pores in the β-SiC contain amorphous carbon as determined by electron energy loss measurements. Excess carbon is needed for sinterability; however, it should be realized that the presence of carbon as a second phase limits the terminal density and may introduce strength-limiting flaws.

5.0 Mechanical Properties

5.1 Deformation Mechanism Mapping for UO_{2+x}

Personnel: D. Knorr, R.M. Cannon and R.L. Coble

An extensive review has been done on the deformation of uranium dioxide where stoichiometric composition has been considered explicitly as a variable. Emphasis has been placed on identifying the basic deformation mechanisms that are operating over the large ranges of stress, temperature, and stoichiometry where the data presented are presumed to be reliable.

The dominant creep behavior at low stresses is concluded to be grain boundary diffusion controlled, contrary to most previous correlations. The major mechanisms in the dislocation glide regime for stoichiometric material are Peierls' glide and a solute mechanism. The solute mechanism is not well characterized either theoretically or experimentally. Little is understood about the dislocation glide of non-stoichiometric urania from a mechanistic standpoint.

Deformation mechanism maps have been constructed at several non-stoichiometric compositions and at several grain sizes at stoichiometric composition. Agreement between the maps and data is good where the deformation field is well characterized. However, many areas are not understood theoretically and/or have not been examined experimentally. This returns to the original caveat of Ashby, who cautioned that the deformation maps are only as good as the theory and the data that are used in their construction.

The maps constructed in this study are the first attempts to consider stoichiometry explicitly as a variable in a ceramic material. The profound effect of composition on deformation behavior in all regimes is graphically evident. Looking at the deformation behavior in toto helps to identify errors in interpretation by individual investigators who usually cover only a small region of the stress-temperature-grain size field in their experiments. At low stresses, the creep rate varies inversely with the grain size cubed, and directly with the deviation from stoichiometry (x).

5.2 Creep in Magnesia-Doped Al_2O_3

Personnel: A.P. Hynes, R.L. Coble and R.M. Cannon

Many studies have been made of the low stress creep behavior of medium and fine-grained alumina. Overall, the stress, grain size and temperature dependencies are fairly consistent with the Nabarro-Herring and Coble

diffusional creep models. At lower stresses and temperatures, evidence exists (R.M. Cannon et al.) of a transition to deformation control by another mechanism.

To examine these effects, a creep apparatus has been constructed for a four-point bend experiment under dead load. Measurement of the deflection rate $\Delta\dot{y}$ = [yc-yl] permits calculation of strain rate independent of the stress component according to $\dot{\epsilon} = 4h\Delta\dot{y}$, where Δy = yc - yl, h is the thickness of the beam sample, yc is the center point, and yl is the load point. Deflection rate (excluding furnace creep) is measured directly by a transducer (DCDT), and is continuously recorded on a chart-recorder for lower stresses. At higher stresses, the transducer output is read directly from a voltmeter. The transducer was calibrated by a micrometer to ±25 μm. Temperature control by a two-variac system maintains a tolerance of approximately ±5°K and up to 1000 watts power are available, although 1723°K is the practical upper limit with the SiC heating elements.

Dense (relative density 97.7%), fine-grained (2.8 to 3.6 μm), tape-cast and sintered alumina was creep tested between 1523°K and 1623°K at stresses between 1.38×10^8 dyne/cm^2 and 6.90×10^5 dyne/cm^2 in an air atmosphere. The total purity was reported as 99.5%, with primary cation impurities of Mg and Si. The total Mg content was between 0.01 and 0.1 weight percent, while the Si content varied between 0.01 and 1.0 weight percent. The MgO content does not appear to be uniform, as evidenced by variability in grain size within one sample set. The saturation limit of MgO in Al_2O_3 has been reported as 0.25 weight percent at 1923°K (Roy and Coble).

The absolute magnitudes of the creep rates measured are lower by up to a factor of four than previously reported creep rates for dense, hot-pressed alumina of similar grain size under similar stress and temperature conditions (R.M. Cannon et al.), and it is believed that this is due to impurity effects. Hot-pressed material has been observed to deform up to an order of magnitude faster than sintered material (W.R. Cannon) at 1923°K. The presence of silica impurity may also have an inhibiting effect on strain rate, since between the two sample sets tested, the one with higher silica content showed a lower creep rate. Additional silica contamination from the SiC heating elements or the insulating furnace firebrick has not been ruled out, although this additional silica did not appear in the semi-quantitative analysis of one crept sample. Slower strain rates may be expected with concurrent grain growth, but comparison of crept and uncrept samples shows only very minor grain growth, insufficient to account for the discrepancies.

Non-viscous behavior ($n > 1$ in $\dot{\epsilon} \propto \sigma^n$) was observed in all cases, as

has been reported in the literature. Although a larger stress range must be tested to precisely determine n, a trend was observed to a slightly higher stress dependence at lower temperatures, up to n = 1.7 at the lowest temperature tested (1523°K or 1250°C). The discrepancy between the observed creep rates and the creep rates predicted by diffusional creep models also increased as the temperature was lowered.

The expected diffusional creep rate was calculated according to the best fit to the previous diffusional creep data determined by R.M. Cannon and R.L. Coble.

$$\dot{\varepsilon} = \frac{14\Omega\sigma}{G^2 kT} D_{eff}$$

where $D_{eff} = D_\ell + \frac{\pi}{G}\delta D_b = \left[1.36\times10^5 \exp\frac{-138\ \text{kcal}}{RT} + \frac{\pi}{G}\, 8.60\times10^{-4} \exp\frac{-100\ \text{kcal}}{RT}\right]$.

Here, $\dot{\varepsilon}$ is the diffusional creep rate, Ω is atomic defect volume taken as 2.1×10^{-23} cm^3, G is the grain size, k is the Boltzmann constant, T is the temperature in degrees Kelvin, and σ is the stress.

This increasing deviation from the diffusional creep models at lower temperatures is consistent with an interface control model where the grain boundaries cannot act as perfect sources or sinks for defects. Burton and Ashby and Verrall have predicted strain rate dependencies of the form $\dot{\varepsilon} \propto M\sigma^2/G$, where M is the mobility of boundary dislocations. Under these conditions, a potential difference must exist between the boundary region and the internal lattice of the grain in order to move a defect, so that energy is absorbed by this interface process and the deformation rate is slowed.

Consistent with the lower creep rates measured, creep activation energies obtained from plots of log $\dot{\varepsilon}TG^2/\sigma$ versus 1/T and calculation of effective diffusivities were found to be higher by almost a factor of two. Diffusion coefficients calculated from the stress-strain data appear to be closer to the aluminum grain boundary coefficients than lattice coefficients.

Correlation of grain size with creep rate will be determined in continuing this work.

5.3 Creep in Tungsten

Personnel: B. Zelinski, R.L. Coble and R.M. Cannon

Small additions of nickel or palladium significantly enhance the sintering rates of tungsten and molybdenum, thus making it possible to obtain very dense materials at low temperatures. These rapid rates are due to

the increased solid state transport of material, but little can be conclusively said at present about the rate-controlling mechanism(s). While a considerable amount of work is being done on the nickel-tungsten system at temperatures above its eutectic (1512°C), little is being done to discern the operative mechanism(s) at lower temperatures. We have designed and built an apparatus to investigate this problem. The apparatus measures very small creep rates (10^{-9}/sec), and through subsequent analysis of the creep data the kinetics of transport can be determined. In general, better theoretical models combined with simpler geometrics make interpretation of creep measurements more productive than performing sintering studies as a source of transport coefficients.

Preliminary creep tests were conducted on tungsten wires to establish equipment reliability and to obtain a data base on tungsten wires with a grain size of about 1 micron at 16,700 psi and temperatures ranging from 1000° to 1400°C. These tests suggested that grain boundary diffusion controlled creep is the operative mechanism at low stresses and temperatures. A subsequent study on the same material at 14,700 psi and temperatures from 100° to 1300°C confirm this conclusion. This second study was conducted after building a water jacket for the apparatus and suitable controls for varying the water temperature. Unfortunately the on-line water temperature itself varies by a few degrees, so a system for monitoring the water jacket temperature is being designed. Work has already been done to construct a monitor to measure the voltage drop across the sample wire. It was found that supply voltage fluctuation caused a significant temperature variation in the wire. This, of course, affects the creep rate as well as the "apparent" sample strain.

When all of the above modifications have been completed, nickel-doped tungsten wires will be studied. In the meantime, various methods to dope the tungsten wire with nickel are being considered. The object will be to obtain a homogeneous doping level as well as the appropriate overall level of $\sim$0.05%. Among the possible techniques are nickel plating, vapor phase equilibration at elevated temperatures, and nickel solution coating with appropriate heat treatments.

6.0 Needs and Opportunities in Ceramic Science

Personnel: W.D. Kingery

We are continuing to devote some effort to the initiative which was taken in the 1975 ERDA conference at M.I.T. on Needs and Opportunities in Ceramic Science; that is, to evaluate and discuss conceptual problems related to ceramic science and ceramic research, how these relate to energy requirements and opportunities, and how they relate to other areas of materials science.

In the past year we have served as a member of the DOE Steering Committee of the Council on Materials Science, participating in discussions to define subjects appropriate for review. The Steering Committee recommended and organized a report on basic research needs in high-temperature ceramics which should be influential in helping to increase the effectiveness of basic research in ceramics related to the objectives of the Department of Energy.

We have prepared a review on energy-related basic ceramic research for the May 1979 International Conference on Modern Ceramic Technologies which was held at St. Vincent, Italy. This review indicates that when a market for technology and a clearly perceived need for new technologies exist, the level of technology rises to the demands of the market. This has been true throughout history. At the present time, all rational analyses of available energy resources and projected new demand indicate a clear need for more efficient energy generation, distribution, conservation and storage, most of which depend on or require the development of new ceramic materials or ceramic materials with special property characteristics. We are entering a period in which the tools available for ceramic research provide the possibility for substantial advances in basic understanding and in development of the means necessary for technological applications. If basic ceramic research is adequately supported and encouraged, it can contribute in a major way towards rational energy technologies; without this support, technological developments will be risky endeavors.

In continuing this activity, we propose to focus on the relationship between grain boundary phenomena and their use in electronic ceramics, an application which has been growing substantially in the last few years in the form of varistor materials, capacitors and other devices closely related to communications and energy distribution applications. We believe that increasing the effectiveness of communication between basic science and its application for these kinds of devices will contribute towards energy effectiveness.

Scientific Staff

1. Senior Staff

	Time Devoted to Research			
W. D. Kingery, Ph.D Professor of Ceramics [redacted]	11/1/79	to 1/31/80	50%	
	7/1/80	to 8/31/80	100%	(2 summer mo
	9/1/80	to 10/31/80	50%	
R. L. Coble, Sc.D Professor of Ceramics [redacted]	11/1/79	to 5/31/80	50%	
	6/1/80	to 6/31/80	100%	(1 summer mo
	8/1/80	to 8/31/80	100%	(1 summer mo
	9/1/80	to 10/31/80	50%	
R. M. Cannon, Jr., Ph.D. Assistant Professor of Ceramics [redacted]	11/1/79	to 5/31/80	10%	
	6/1/80	to 6/31/80	20%	(1 summer mo
	8/1/80	to 8/31/80	20%	(1 summer mo
	9/1/80	to 10/31/80	10%	

Professors Kingery and Coble continued as Principal Investigators. In all cases, the research programs are organized, planned and carried out in close consultation with the Principal Investigators.

2. Graduate Students and Research Staff

J. Blendell
J. Blum
K. Cheng
W. Coblenz
N. Dudney
J. Dynys
T. Gattuso
E. Giraldez
C. Handwerker
A. Hneriksen
A. Hynes
K. Kijima
N. Mizutani
D. Sempolinski
Y. Tajima
W. Westphal
S. T. Wu
T. Yager
B. Zelinski

UROP Student - Y. M. Chang

3. Support Staff

Secretaries 2
Technician 1
Administrative Assistant 1
Research Associates 3

4. Other Support by Federal Agencies Involving Senior Staff

W. D. Kingery	None		
R. L. Coble	None		
R. M. Cannon, Jr.	25%	NSF	5/1/79 to 4/30/80
	15%	DOD	7/1/79 to 6/30/80

We plan that all directly identified ceramic research and the entire research support of Professors Kingery and Coble continue to be provided by this contract and that no support of other agencies be solicited. There is no technical overlap between present contract work and that funded by the other government contracts.

5. Awards

Professor Coble was nominated as the Sosman Lecturer, 1979, of the Basic Science Division, American Ceramic Society. He was also Visiting Scientist and Guest Lecturer at the Max Planck Institute for Metallurgy, Stuttgart, for approximately one month during the past year.

6.0 Publications

6.1 Theses

J. E. Blendell, "The Origins of Internal Stresses In Polycrystalline Al_2O_3 and Their Effects on Mechanical Properties," Sc.D., M.I.T. Department of Materials Science and Engineering, June 1979

J. B. Blum, "The Vacuum Ultraviolet Properties of Aluminum Oxide and Their Relation to the Electrical Conductivity," Ph.D., M.I.T., Department of Materials Science and Engineering, September 1979

N. J. Dudney, "The Electrical Properties of Pure and Yttria Doped Uranium Dioxide," Ph.D., M.I.T., Department of Materials Science and Engineering, September 1979

D. R. Sempolinski, "The High Temperature Electrical Properties of Single Crystalline MgO,", Sc.D., M.I.T., Department of Materials Science and Engineering, June 1979

6.2 Papers published or accepted for publication

John R. H. Black and W. D. Kingery, "Segregation of Aliovalent Solutes Adjacent Surfaces in MgO," Journal of the American Ceramic Society 62 (3-4), 176-8 (1979).

J. E. Blendell and R. L. Coble, "Test by Numerical Simulation of Applicability of Steady State Diffusion Models in Final Stage Sintering," Powder Metallurgy International, Vol. 10, No. 2, 1978

R. L. Coble, "Hot Consolidation of Rapidly Solidified powders: Sintering Hot Pressing (PH) and Hot Isostatic Pressing (HIP) in Relation to the Superalloys," Powder Metallurgy International, 10, 3 August, 1978

W. H. Gourdin and W. D. Kingery, "The Defect Structure of MgO Containing Trivalent Cation Solutes: Shell Model Calculations," Journal of Materials Science, in press.

W. H. Gourdin, W. D. Kingery and J. Driear, "The Defect Structure of MgO Containing Trivalent Cation Solutes: The Oxidation-Reduction Behavior of Iron," Journal of Materials Science, in press

A. F. Henriksen and W. D. Kingery, "The Solid Solubility of Sc_2O_3, Al_2O_3, Cr_2O_3, SiO_2 and ZrO_2 in MgO, "Ceramurgia International 5 (1), 11-17 (1979)

A. F. Henriksen and W. D. Kingery, "Effects of Strain Energy on Precipitate Morphology in MgO," Ceramurgia International, in press.

W. D. Kingery, J. B. Vander Sande and Takashi Mitamura, "A Scanning Transmission Electron Microscopy Investigation of Grain-Boundary Segregation in a ZnO-Bi_2O_3 Varistor," Journal of the American Ceramic Society 62 (3-4), 221-2 (1979).

W. D. Kingery, T. Mitamura, J. B. Vander Sande and E. L. Hall, "Boundary Segregation of Ca, Fe, La and Si in MgO," Journal of Materials Science, in press.

W. D. Kingery, "Solute Segregation and Precipitation Phenomena in Oxide Ceramics," Ceramics Japan 14 (6), 548 (1979). In Japanese.

W. D. Kingery, "Energy-Related Basic Ceramic Research," to be published in Proceedings of the 4th CIMTEC (International Meeting on Modern Ceramic Technologies), St. Vincent, Italy, May 28 - June 1, 1979.

W. D. Kingery, "Interactions of Ceramic Technology with Society," abstracted in part from the 1978 Jacob Kurtz Memorial Lecture, Technion, Haifa, Israel; to be published in P. Rice (ed.), Matson festschrift.

T. Mitamura, E. L. Hall, W. D. Kingery and J. B. Vander Sande, "Grain Boundary Segregation of Iron in Polycrystalline Magnesium Oxide Observed by STEM," Ceramurgia International, in press.

Y. Moriyoshi, W. D. Kingery and J. B. Vander Sande, "Dislocation Motion in Magnesium Oxide," Journal of Materials Science 13, 2507-10 (1978)

C. F. Yen and R. L. Coble, "Defect Centers in Gamma-Irradiated Single-Crystal Al_2O_3," Journal of the American Ceramic Society, Vol. 62 No. 1-2 Jan-Feb., 1979

6.3 Papers submitted for publication

None

6.4 Lectures or papers presented or scheduled

W. D. Kingery, "Energy-Related Basic Ceramic Research," Keynote Address, 4th CIMTEC (International Meeting on Modern Ceramic Technologies) St. Vincent, Italy, May 28 - June 1, 1979.

W. D. Kingery, "Discussion," presented at the Seminar on Early Pyto-technology, Smithsonian Institution, Washington, D.C., April 19-20, 1979

Papers presented at the Annual Meeting of the American Ceramic Society, Cincinnati, Ohio, April 29 - May 2, 1979

R. L. Coble, "On The Sintering Behaviors in Chemically Reactive Systems," Sosman Memorial Lecture

J. E. Blendell and R. L. Coble, "Measurements of Residual Stresses in Al_2O_3 due to Thermal Expansion Anisotropy"

J. E. Blendell and R. L. Coble, "Effect of heating Rate on the Interpretation of Initial Sintering Data"

J. B. Blum, H. L. Tuller and R. L. Coble, "Temperature Dependence of the Bank Gap of Ionic Crystals"

W. S. Coblenz, R. L. Coble and R. M. Cannon, "Influence of Boron on the Vapor-Transport Rate of Silicon"

N. J. Dudney, R. L. Coble and H. L. Tuller, "Charge Transport and Kinetic Properties of Pure and Y_2O_3-Doped UO_{2+x}"

J. M. Dynys, R. L. Coble and R. M. Cannon, "Initial-State Sintering Mechanisms in Al_2O_3"

D. R. Sempolinski and W. D. Kingery, "High Temperature Electrical Properties of MgO"

T. A. Yager and W. D. Kingery, "Complex Clustering of Trivalent Cationic Impurities in MgO"

T. A. Yager and W. D. Kingery, "Laser-Heated High Temperature EPR Spectroscopy"